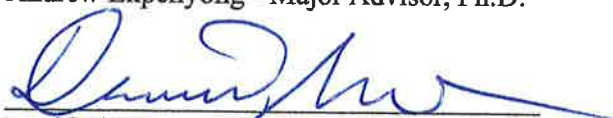


THESIS APPROVED BY

August 17, 2018
Date



Andrew Ekpenyong - Major Advisor, Ph.D.



David Sidebottom - Committee Member, Ph.D.

Patricia Soto

Patricia Soto - Committee Member, Ph.D.



Gail M. Jensen, Ph.D., Dean

OPTO-ELECTRONIC MODULATION OF QUANTUM DOTS BY CELLS AND BIOACTIVE MOLECULES

by

BONG HAN LEE

A THESIS

Submitted to the faculty of the Graduate School of Creighton
University in Partial Fulfillment of the Requirements for the degree of
Master of Science in Physics in the Department of Physics

Omaha, NE
August 22, 2018

Abstract

Quantum dots (QDs) have applications and promising myriad applications in photovoltaic cells, biomedical imaging, targeted drug delivery, and quantum information processing. These have led to much research on their interactions with other systems. For biological systems, research has focused on the biocompatibility and cytotoxicity of QDs in the context of imaging/therapy. However, there is a paucity of work on how biological systems and bioactive molecules might be used to alter the opto-electronic properties of QDs.

Here, we show that these properties can be altered by bioactive molecules and biological macromolecules following controlled changes in cellular activities. Using CdSe/ZnS core/shell QDs, spectroscopic analysis of optically excited colloidal QDs with HL60, K562, and T98G cell lines are performed. Our results show statistically significant ($p < 0.001$ and $p < 0.0001$) quenching of the emission spectra of the colloidal dispersions due to bioactive molecules in common chemotherapeutic drugs and due to reactive oxygen species (ROS) produced by these cells (HL60, K562) following chemotherapy and radiotherapy. This optical modulation constitutes what we describe as opto-electronic modulation. This type of tuning will possibly enhance applications of QDs in green energy and biomedical imaging.

Acknowledgments

This thesis would have not been completed without the support of caring, intelligent, and experienced individuals. I thank Dr. Andrew Ekpenyong, my advisor, for being very supportive of my career goals and for preparing me as no one else did so that I can reach those goals on my own. Thank you for pointing out to the night sky to make me realize of the the vastness of discoveries that are yet to be made. If I would have not worked under your guidance, I would have been “blinded”. I thank my thesis committee members, Dr. David Sidebottom and Dr. Patricia Soto for their efforts in seeing this thesis completed, and for being quintessential models of a scientist. I thank the Translational Biomedical Physics (TBP) research lab members for their collaboration with my research. I thank Creighton faculty and staff Dr. Baruth, Dr. Wong, Dr. Nichols, Mr. Brad Walters for providing technical information in their area of expertise and critical questioning. I thank Creighton students Laura Aumen for troubleshooting my work in LaTeX, and Tomilola Obadiya, Amrit Gautam, Matt Butchek, and Vy N Do for hearing my oral practice presentations of this thesis. Lastly, I am forever in indebted to the Creighton Physics Department as it has been the birthplace of my purpose of life.

To Dad

Contents

Abstract	iii
Acknowledgments	iv
Dedication	v
1 Introduction	1
1.1 What are QDs?	1
1.2 How are QDs Made?	3
1.3 How do QDs Work?	5
1.4 Quantum Mechanics of QD	8
1.4.1 Quantum Confinement	8
1.4.2 Schrödinger Equation	9
1.4.3 Energy Eigenvalues	11
1.5 Biomedical Applications of QD	13
1.5.1 Cell Induced or Bioactive-Molecule-Induced Opto-Electronic Mod- ulation of QD	15
2 Computational Methods	16
2.1 COMSOL Multiphysics 5.3	16
2.1.1 Simulation Workflow	17
2.1.2 Statistical Methods	24

3	Experimental Methods (Spectroscopy)	25
3.0.1	Materials	25
3.0.2	Methods	30
3.0.3	Statistical Methods	33
4	Results	35
4.1	Computational Results	35
4.2	Spectroscopic Results	36
4.2.1	Hydrophobic and Hydrophilic QDs Alone	36
4.2.2	Hydrophobic and Hydrophilic QDs with Hydrogen Peroxide	39
4.2.3	Hydrophilic QDs with Bioactive Molecules and Cells	41
5	Discussion and Conclusions	49
5.1	Discussion	49
5.1.1	QD Opto-Electronic Properties Simulated in COMSOL Multi-physics	49
5.1.2	Fluorescence Intensity Modulation of QDs with Hydrogen Peroxide	50
5.1.3	Bioactive Molecules Alter Opto-Electronic Properties of QDs	50
5.1.4	Molecules from Cells During Chemotherapy Modulate QD Fluorescence	51
5.1.5	Molecules from Cells Post-Radiotherapy Modulate QD Fluorescence	52
5.1.6	Simulations of Possible Mechanisms	53
5.1.7	Limitations and Suggestions for Future Experiments	57
5.1.8	Conclusions	57
A	Published Abstracts	59

B Published/Submitted Journal Articles	65
C Cell Culture Protocols	66
D Spectroscopic Protocols	70
E COMSOL Codes	74
F Copyright Permissions	77
G List of Experiments	81
References	83

List of Tables

2.1	Simulation Parameters.	21
3.1	Experimental Conditions.	31
4.1	Energy Eigenvalues of the Electron in CdSe/ZnS QD Well.	36
4.2	Energy Eigenvalues of the Hole in CdSe/ZnS QD Well.	36
4.3	Experimental Conditions Outcome.	48
G.1	Complete List of Experimental Conditions.	82

List of Figures

1.1	Periodic Table for Semiconductor Elements.	2
1.2	Composite QD.	3
1.3	Colloidal CdSe/ZnS QDs.	4
1.4	Energy Band Diagram.	6
1.5	Energy Band Structure of QDs.	7
1.6	Potential Wells.	11
1.7	Composite CdSe/ZnS QD.	14
2.1	Flow Chart of the Simulation Workflow.	18
2.2	Geometry of QD.	19
2.3	Dirichlet Boundary Conditions on QD.	22
2.4	Composite QD with FEM.	23
2.5	Probability Density in COMSOL Multiphysics 5.3.	23
3.1	Spectroscopic Equipment.	26
4.1	Hydrophobic CdSe/ZnS QD Spectra.	37
4.2	Hydrophilic CdSe/ZnS QD Spectra.	38
4.3	Spectra and Statistical Comparison for Hydrophobic CdSe/ZnS QD with H_2O_2	39
4.4	Spectra and Statistical Comparison for Hydrophilic CdSe/ZnS QD with H_2O_2	40

4.5	Spectra and Statistical Comparison for Hydrophilic CdSe/ZnS QD with H_2O_2	41
4.6	Spectra and Statistical Comparison for HL60 Cells Treated with Chemotherapy Drugs.	42
4.7	Spectra and Statistical Comparison for K562 Cells Treated with Chemotherapy Drugs.	43
4.8	Spectra and Statistical Comparison for HL60 Cells Treated with Radiotherapy.	44
4.9	Spectra and Statistical Comparison for K562 Cells Treated with Radiotherapy.	45
4.10	Spectra and Statistical Comparison for T98G Cells Treated with Radiotherapy (N1).	45
4.11	Spectra and Statistical Comparison for T98G Cells Treated with Radiotherapy (N2).	46
4.12	Spectra and Statistical Comparison for T98G Cells Treated with Radiotherapy (N3).	47
5.1	First Possible Mechanism.	54
5.2	Second Possible Mechanism.	55
5.3	Third Possible Mechanism.	56

Chapter 1

Introduction

1.1 What are QDs?

QDs are semiconductor nanoparticles that are in the size range of 1 – 20 nm, where a single QD can be made from up to 10,000 atoms [11]. These nanoparticles were discovered by Alexei Ekimov while studying semiconductor-doped glasses in the 1980s, but were first published by Louis Brus in 1984 [28] [18] [17]. Over the years, QDs have been tailored with combinations of semiconductor elements and physical properties (geometry, shape, and size) for applications. In this research, we utilized CdSe/ZnS core/shell semiconductor nanoparticles for biological applications explained further in section 1.5.

To form a semiconductor material from several elements, the octet rule needs to be fulfilled to form covalent bonds; exceptions to the octet rule exist when bonds are strongly covalent or are ionic compounds [21]. Figure 1.1 shows the possible combination of elements to form semiconductor materials such as CdSe and ZnS. To fabricate composite CdSe/ZnS core/shell QDs, we introduce the colloidal synthesis technique.

	III	IV	V	VI
	5 B	6 C	7 N	8 O
II	13 Al	14 Si	15 P	16 S
30 Zn	31 Ga	32 Ge	33 As	34 Se
48 Cd	49 In	50 Sn	51 Sb	52 Te
80 Hg	81 Tl	82 Pb	83 Bi	84 Po

Figure 1.1: **Periodic Table for Semiconductor Elements.** To fulfill the octet rule, elements in the periodic table are combined to create semiconductor elements. The roman numbers indicate the number of valence electrons of each element. The color coding of the columns shows the possible combination of elements to form semiconductor materials (II-VI, III-V, and IV-IV).

1.2 How are QDs Made?

Colloidal synthesis nucleates semiconductor elements up to a desired size at specified temperatures, concentrations and times [25]. A typical composite QD is shown in Figure 1.2, and a sample of colloidal QDs is shown in Figure 1.3. The choice of elements and fabrication method of QDs contribute to the optical and electronic (opto-electronic) properties of QDs. Hence, we present these properties in the context of how QDs work.

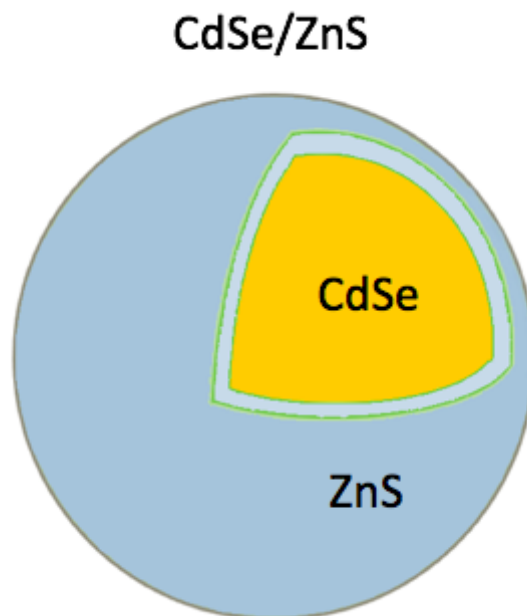


Figure 1.2: **Composite QD.** Semiconductor elements from group II-VI form the CdSe core and elements from group II-VI form the ZnS shell.

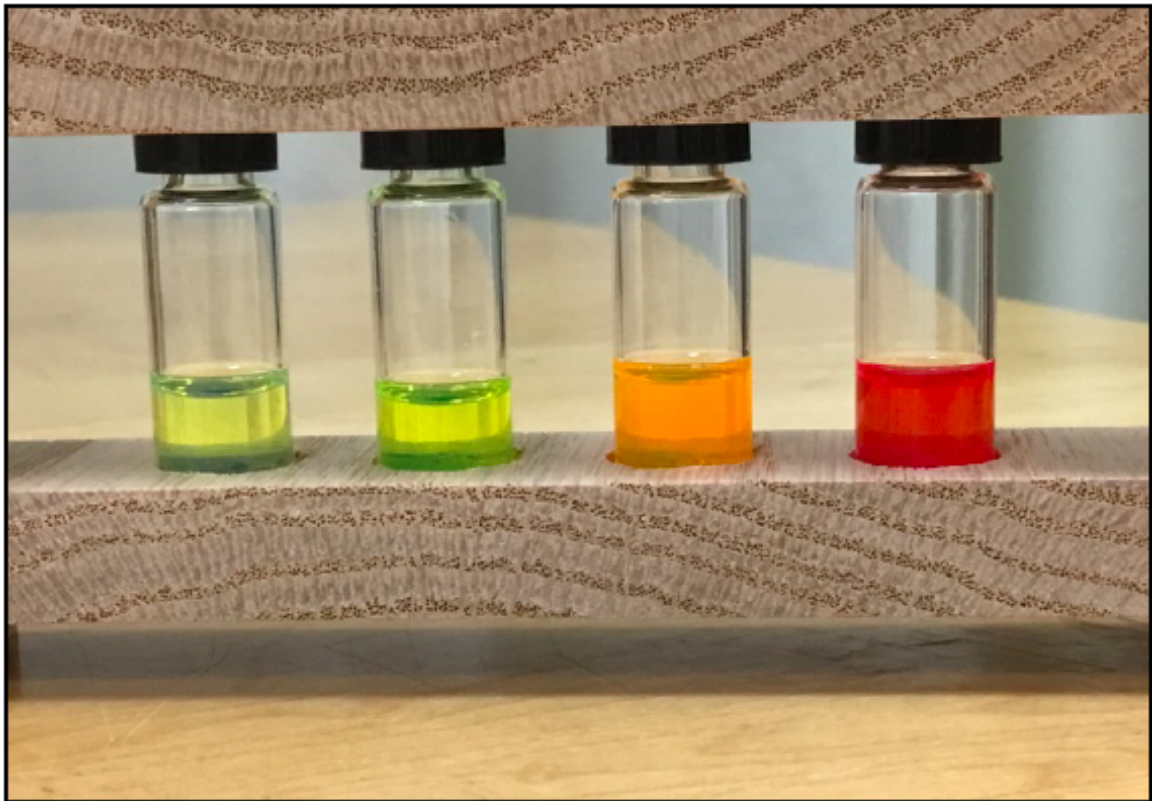


Figure 1.3: Colloidal CdSe/ZnS QDs. Colloidal QD size increases from left to right.

1.3 How do QDs Work?

As a basis, we describe the opto-electronic properties of QDs using the energy band diagram for bulk semiconductor materials as shown in Figure 1.4. In the energy band diagram, energy bands represent the collection of individual energy levels of electrons' bound states from atoms. The highest energy band occupied by electrons is called the valence band. The energy band above the valence band is the conduction band. These two bands characterize the opto-electronic properties of bulk semiconductor materials. When photons and thermal energy excite electrons from the valence band to the conduction band, excited electrons leave holes in the valence band, indicating the unfilled regions in the valence band. These electron-hole pairs become known as carriers.

If the energy supplied is equal to the energy band gap, carriers recombine emitting a photon with an energy equal to the energy band gap. If the energy supplied is higher than the energy band gap, carriers release energy thermally via lattice vibrations reaching to their respective band gap edges. These carriers then recombine releasing a photon with an energy equal to the energy band gap. The latter scenario is possible because energy bands are a continuum of discrete energy levels [21].

Unlike energy bands from bulk semiconductor materials, QDs possess discrete energy levels that do not form a continuum and change in a size-dependent manner. These properties make smaller QDs emit shorter wavelength photons and larger QDs emit longer wavelength photons as shown in Figure 1.5. Moreover, a highly energetic photon causes the excited electron to possess excess kinetic energy. This electron collides with other bound electrons to create additional electron-hole pairs [64] [39], contributing to the QDs' highly photoluminescence properties. Because QDs confine

charge carriers due to their size, we incorporate quantum mechanics to understand fully the opto-electronic properties of QDs.

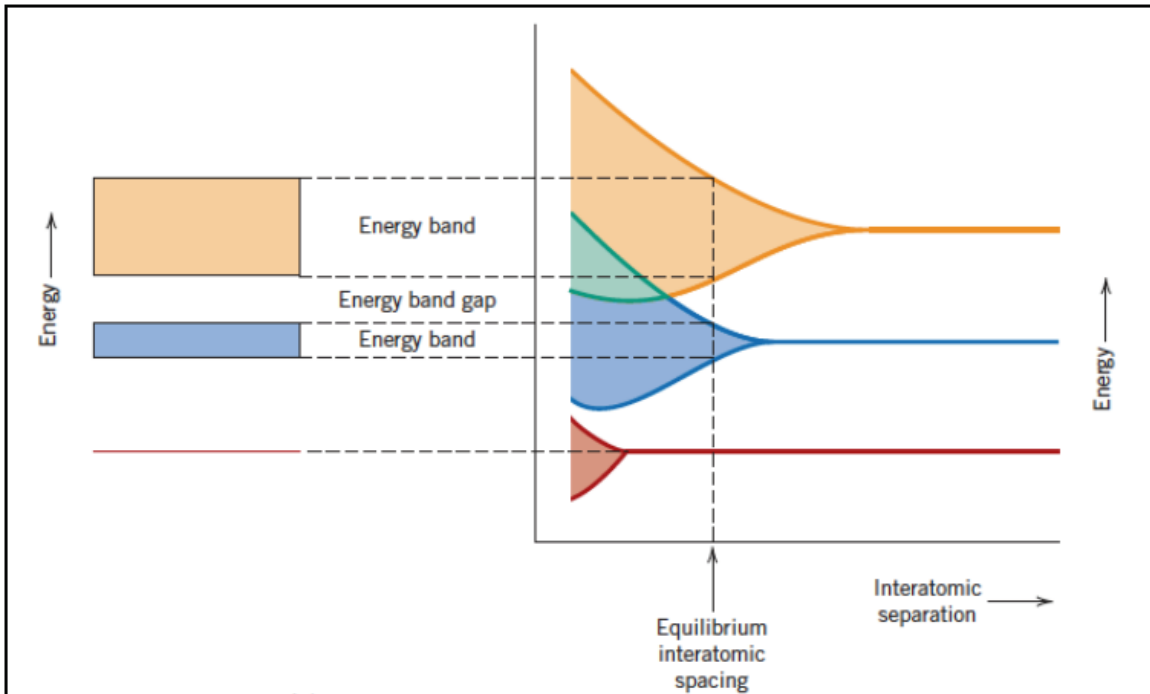


Figure 1.4: **Energy Band Diagram.** As the interatomic separation of atoms becomes smaller, atoms perturb each other to split energy levels (right) and to form energy bands at the equilibrium interatomic spacing separated by an energy band gap (left). Higher energy levels split first as they are further away from the atom's nucleus as shown in yellow and blue. The lowest energy level does not form an energy band at equilibrium interatomic spacing as it is closest to the nucleus as shown in red. (See appendix F for documentation of permission to republish this material from [21].)

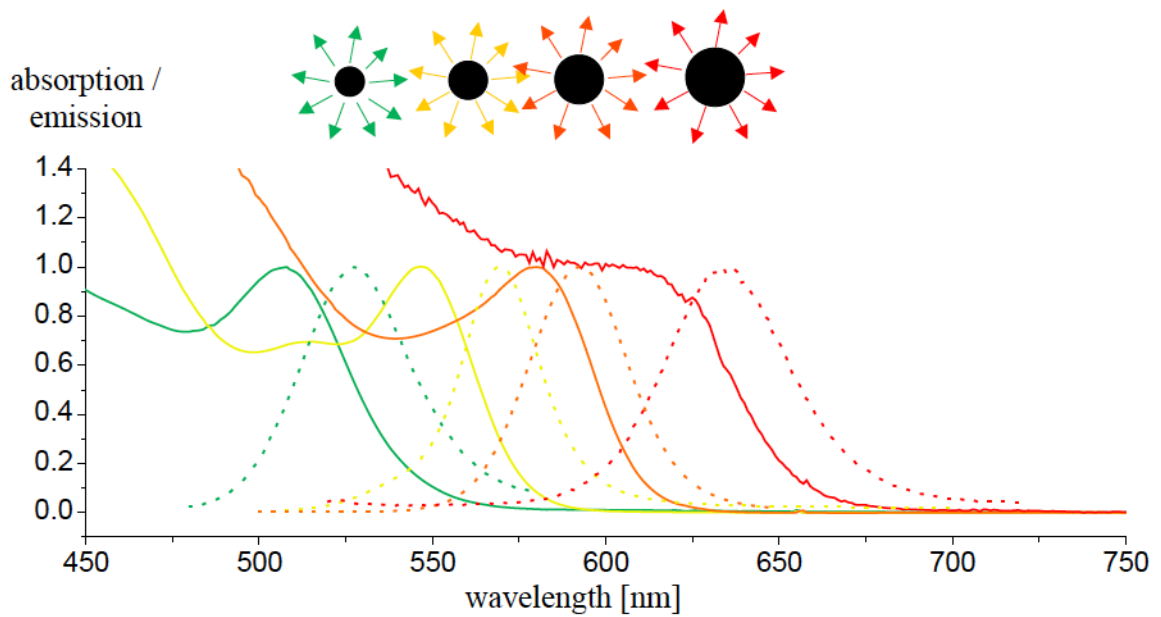


Figure 1.5: **Emission Spectra of QDs.** From this absorption/emission (arbitrary light units, a.u.) vs wavelength (nm) plot, the photon wavelength absorbed and emitted is inversely proportional to the energy difference between the bound states. From smaller to larger QDs (left to right), QDs absorb from higher to lower energies (solid lines). Analogously, the emission spectra (dotted lines) shows QDs emitting from higher to lower energy photons (left to right). (See appendix F for documentation of permission to republish this material from [63].)

1.4 Quantum Mechanics of QD

Semiconductor theory describes the bulk material properties of QDs. However, the theory fails to completely address some of the opto-electronic properties of QDs. Thus, to adequately describe the physical behavior of QDs, we incorporate quantum mechanics to understand better their opto-electronic properties of QDs [58] [64]. Understanding these properties will give us the reason why the energy band gap is inversely proportional to the wavelength of the QD's photoluminescence; a property defined by quantum confinement [15]. Moreover, these properties will be analyzed mathematically using the Schrödinger equation [63].

1.4.1 Quantum Confinement

Quantum confinement can be analogously described with the particle confined in a box and Heisenberg's uncertainty principle. As the particle moves in the box, the particle is restricted to move at a certain velocity. This velocity is obtained from the momentum term of the Heisenberg's uncertainty principle as shown in equation (1.1). Using this idea, the size-dependent wavelength of QDs from section 1.3 can be explained by treating the QD as the box.

$$\Delta x \Delta p \geq \frac{h}{2\pi}, \quad (1.1)$$

where x is the position, p is the momentum, and h is Planck's constant.

As the box confining the particle becomes smaller, Δx decreases, and Δp increases by the inequality relation in equation (1.1); larger values of momentum indicate a more energetic particle, leading to a smaller emission wavelength. Similarly, as the box confining the particle becomes larger, Δx increases, making Δp to decrease; smaller values of momentum indicate less energetic particle, leading to a larger emission wave-

length. The Schrödinger equation provides such behavior with more mathematical detail.

1.4.2 Schrödinger Equation

As Newton's laws are for classical mechanics, and Maxwell's equations are for electromagnetism, the Schrödinger equation is for quantum mechanics. The Schrödinger equation describes the behavior of matter at the nuclear, atomic, and molecular scales. This behavior is expressed as waves (wavefunctions). These wavefunctions locate particles in space, and yield the energy levels of the quantum mechanical system [70]. We write the Schrödinger equation as

$$\hat{\mathcal{H}}\psi = E\psi, \quad (1.2)$$

where $\hat{\mathcal{H}}$ is the Hamiltonian, a mathematical operator, of the system, ψ is the wavefunction of the particle, and E is the total energy of the system. The Hamiltonian is expressed in terms of the kinetic and potential energy of the quantum mechanical system where $\hat{\mathcal{H}} = -\frac{\hbar^2}{2m}\nabla^2 + V$ is substituted into equation (1.2) making

$$-\frac{\hbar^2}{2m}\nabla^2\psi + V\psi = E\psi. \quad (1.3)$$

Since QDs are semiconductor materials, we consider the mass, m , of the electron and hole, and their respective effective masses are also considered [63]. The Laplacian operator, ∇^2 , uses different coordinate systems (cartesian, polar, cylindrical, and spherical) to fit physical parameters. We treat the QD as a sphere [63], and express the Laplacian operator in spherical coordinates as shown in equation (1.4):

$$\nabla^2 = \left(\frac{1}{r^2}\frac{\partial}{\partial r}\left(r^2\frac{\partial}{\partial r}\right)\right) + \frac{1}{r^2\sin(\theta)}\frac{\partial}{\partial\theta}\left(\sin(\theta)\frac{\partial}{\partial\theta}\right) + \frac{1}{r^2\sin^2(\theta)}\left(\frac{\partial^2}{\partial\phi^2}\right). \quad (1.4)$$

Thus, equation (1.3) is modified to provide the time-independent Schrödinger equation in spherical coordinates [33]:

$$\frac{-\hbar^2}{2m_e} \left[\left(\frac{1}{r^2} \frac{\partial}{\partial r} \left(r^2 \frac{\partial}{\partial r} \right) + \frac{1}{r^2 \sin(\theta)} \frac{\partial}{\partial \theta} \left(\sin(\theta) \frac{\partial}{\partial \theta} \right) + \frac{1}{r^2 \sin^2(\theta)} \left(\frac{\partial^2}{\partial \phi^2} \right) \right) \right] \psi + V\psi = E\psi. \quad (1.5)$$

Using equation (1.5), the energy eigenvalues are calculated.

1.4.3 Energy Eigenvalues

Just like the energy eigenvalues for a particle in a box, one can calculate the energy eigenvalues of QDs in an infinite QD well as shown in Figure 1.6.

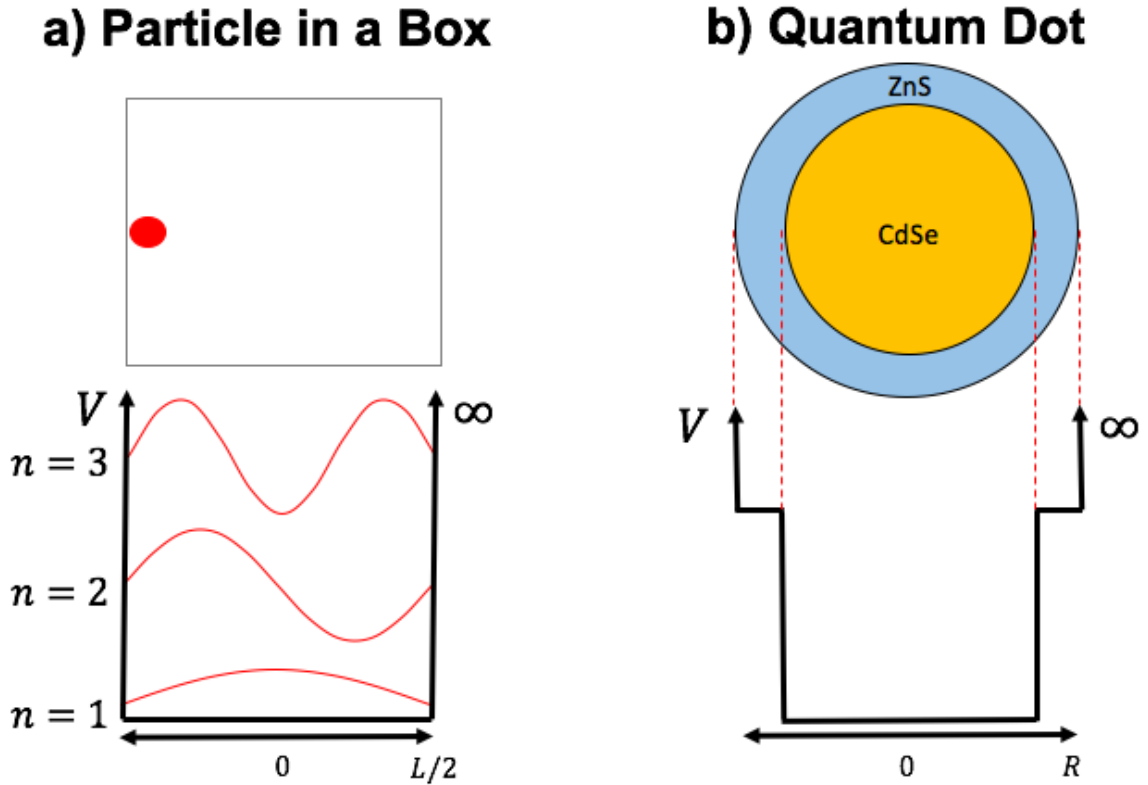


Figure 1.6: **Potential Wells.** (a) the 1D infinite square well of a particle (red) confined in a box. The three lowest energy eigenvalues are shown. (b) the 1D infinite of CdSe/ZnS QD potential well. The infinite QD well differs by the changing potentials that are associated with the QD's material properties.

The resulting energy eigenvalue for a QD results to be

$$E_n = \frac{h^2 n^2}{8md^2}, \quad (1.6)$$

where d is the diameter of the QD, and n is the principal quantum number, which are integer numbers (1, 2, 3, and onwards).

There are multiple energy eigenvalues for an infinite potential. These energy eigenvalues are defined by the n integer term in equation (1.6). We use the lowest energy eigenvalue ($n = 1$) of the electron and hole when calculating for the energy difference of the emission [5] [63]. In addition to these energy eigenvalues, the energy band gap, E_g , and Coulombic potential term, E_c , between the electron and hole are accounted to calculate for the energy difference, ΔE .

$$\Delta E = E_g + E_{n_e} + E_{n_h} + E_c \approx \frac{hc}{\lambda}, \quad (1.7)$$

where E_{n_e} is the energy level of the electron, and E_{n_h} is the energy level of the hole.

We express the terms of equation (1.7) in the following manner:

1. E_g is typically the value obtained from a bulk semiconductor material. However, for QDs, one chooses the E_g of the confined region of the carriers. In the case of CdSe/ZnS, carriers are confined in the core, CdSe. Thus, we use E_g for CdSe (1.74 eV [12]).
2. Equation (1.6) is modified for E_{n_e} and E_{n_h} . Since semiconductor materials are being used, we consider their effective masses. For E_{n_e} ,

$$E_{n_e} = \frac{h^2}{8m_e^*d^2}, \quad (1.8)$$

where m is modified for the effective mass of the electron, m_e^* . Similarly, for E_{n_h} ,

$$E_{n_h} = \frac{h^2}{8m_h^*d^2}, \quad (1.9)$$

where m is modified for the effective mass of the hole, m_h^* .

3. E_c is expressed as

$$E_c = \frac{ke^2}{d_{eh}}, \quad (1.10)$$

where e is the charge of the electron, k is the Coulomb's law constant, and d_{eh} is the distance wherein the carriers are confined.

Using these terms, we express equation (1.7) as

$$\Delta E = E_g + \frac{h^2}{8m_e^*d^2} + \frac{h^2}{8m_h^*d^2} - \frac{e^2}{8\pi\epsilon d_{eh}} \approx \frac{hc}{\lambda}. \quad (1.11)$$

With these opto-electronic properties of QDs, we extend to understand their application in the biomedical context.

1.5 Biomedical Applications of QD

For biological applications, QDs label biological molecules and cells for targeted imaging [50]. Compared to organic dyes and fluorescent proteins, QDs surpass their photoluminescence properties [67]. To attach QDs to biological molecules and cells, surface reactants are integrated onto the QDs' shell as shown in Figure 1.7 [48].

Although most publications focused on the biocompatibility of QDs in the context of imaging/therapy [67] [55], there have been a paucity of work on how biological systems might be used to modulate the opto-electronic properties of QDs. To investigate how this opto-electronic modulation occurs, computational simulations and spectroscopic experiments were done to explore cell induced or bioactive-molecule-induced opto-electronic modulation of QD.

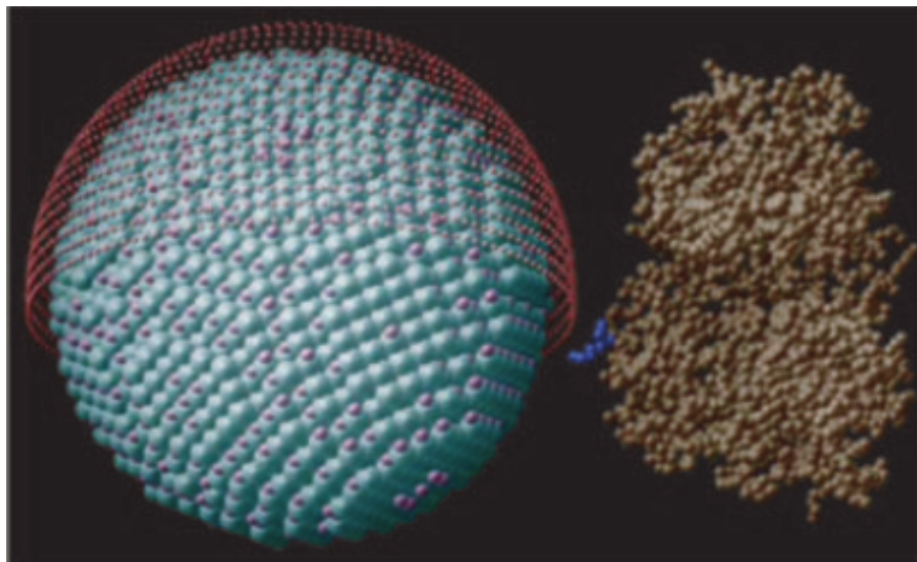


Figure 1.7: **Composite CdSe/ZnS QD.** At the left is a composite QD with two different QDs (CdSe as cyan and ZnS as purple) and are covered with dihydrolipoic acid (pink), a surface reactant that is used so that the composite QD can attach to biomolecules. The biomolecule shown at the right is MBP, a midsize protein. (See appendix F for documentation of permission to republish this material from [48].)

1.5.1 Cell Induced or Bioactive-Molecule-Induced Opto-Electronic Modulation of QD

Prior to investigating the cell induced or bioactive-molecule-induced modulation of QD, we wonder of the possible types of opto-electronic modulation in the context of biomedical applications.

Few studies of photoluminescence properties from QDs in living cells have been reported so far [71]. In this investigation, we emphasize the photoluminescence properties of QDs in living cells after these cells have been treated with chemotherapy and radiotherapy. These treatments make changes in the amount of reactive oxygen species (ROS) to target cancer cells [59].

ROS are partially reduced oxygen molecules that are highly reactive due to their unpaired electrons [59]. These molecules are formed when oxygen derived molecules gain electrons, and interact with other molecules such as super-oxide dismutase (SOD) generated by cells. This interplay leads to ROS in different forms such as hydrogen peroxide (H_2O_2), superoxide radical (O_2^-), hydroxyl radical (OH^-) and hypochlorous acid ($HClO$) [30]. With this interplay, ROS ensure cellular homeostasis and signaling [27]. However, ROS in excess lead to alterations to lipids, proteins and DNA, leading to aging and diseases [27]. Despite the adverse effects of ROS, they are important for chemotherapy and radiotherapy.

Experiments involving ROS and their effects onto the photoluminescence changes of QDs have been already reported [71] [31] [47]. The effect of ROS and other partially reduced molecules in the context of chemotherapy and radiotherapy are of interest as there are cell induced or bioactive-molecule-induced participating in the process as well. Prior to a spectroscopic study, we model the QD via computer simulation.

Chapter 2

Computational Methods

2.1 COMSOL Multiphysics 5.3

COMSOL Multiphysics 5.3 Software was used to simulate the opto-electronic properties of QDs including their energy eigenvalues. COMSOL is a commercially available higher level language software platform built from Java and MATLAB languages, and Graphical User Interface (GUI) [3]. The software performs advanced numerical methods to model, and simulates physics based problems. Moreover, the software serves as a platform to couple different physical phenomena to unify a step by step workflow of electrical, mechanical, fluidic, thermal, and mathematical applications.

COMSOL is an equation-based modeling software. Thus, the user implements parameters and geometries for an equation-based modeling based on partial differential equations (PDE). The Schrödinger equation is a PDE, and this enables us to use COMSOL in solving it for QDs. Since most PDEs possess numerical solutions [1], Finite Element Method (FEM), a method of approximating solutions of PDEs numerically [44], was used. For the case of the composite QD, the Schrödinger equation in spherical coordinates, as shown in equation (1.5), was transformed into its

coefficient form. This transformation simplifies the simulation workflow that will be used to obtain the energy eigenvalues of the QD [14][49]. One of the advantages in FEM is that the degree of discretization is freely chosen. However, the degree of discretization depends on the PDE being solved, and limited by computer resources [4]. All simulations of COMSOL Multiphysics 5.3 were run on Intel(R) Core(TM) i5-250M CPU at 2.50 GHz using 2 cores on 1 socket. The available memory of the computer was 3.98 GB. In order to proceed to the simulation, we inputted parameters in a step by step process.

2.1.1 Simulation Workflow

The simulation workflow consisted of seven steps. A flow chart of the simulation workflow is shown in Figure 2.1.

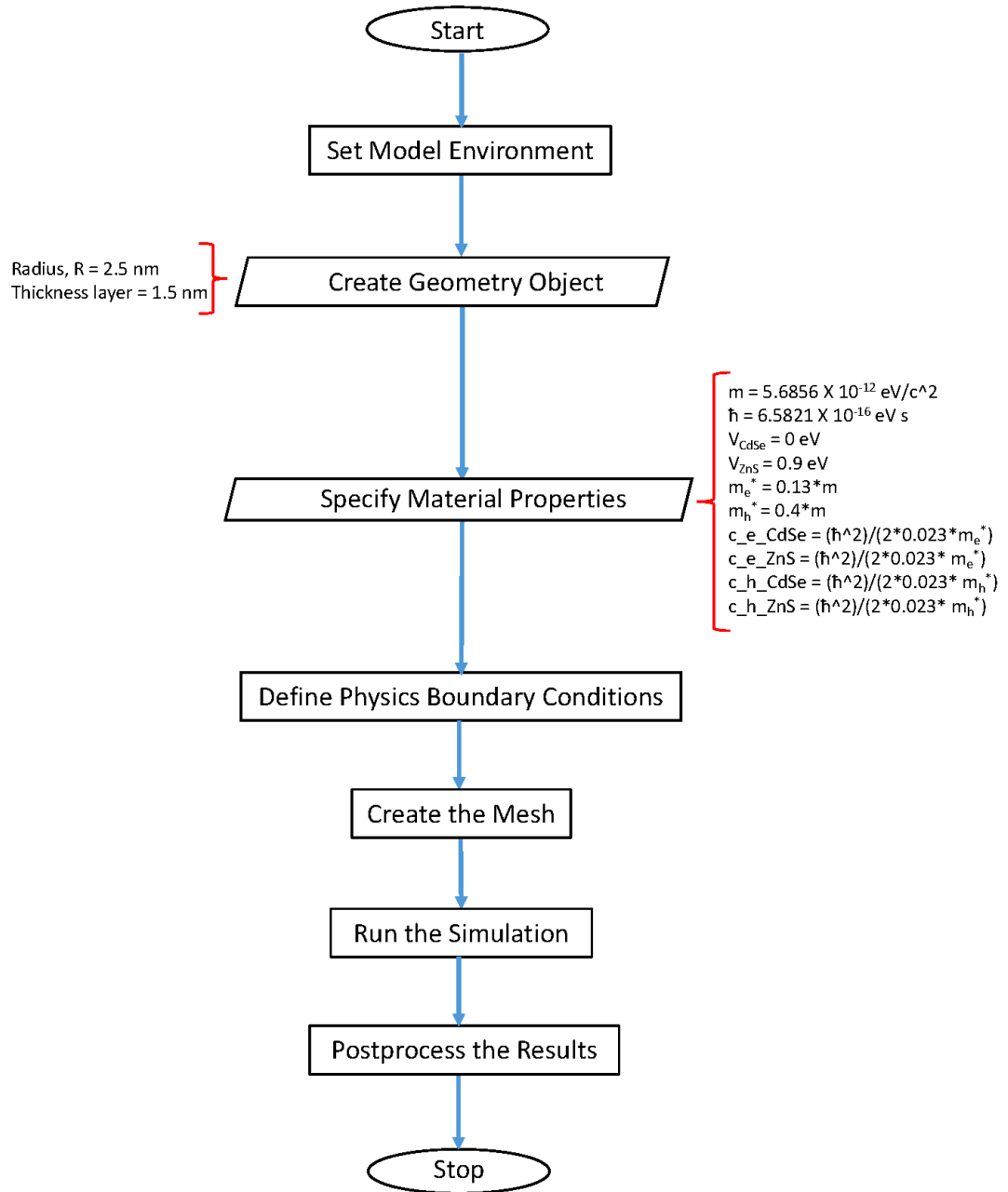


Figure 2.1: **Flow Chart of the Simulation Workflow.** Steps 1 through 7 of the simulation workflow is shown with the respective input parameters gathered from Table 2.1.

Step 1: Set Up Model Environment The user sets up the model environment by choosing spatial dimension (3D, 2D, 1D Axisymmetric, or 0 D), type/s of physics (Electromagnetics, Structural, Acoustics, Fluid, Heat and Mathematics), and study type consisting of a solver for the computation. For the composite CdSe/ZnS QD, a 3D study was made. Mathematics was used since a quantum mechanical type of physics is not provided in COMSOL [49]. In Mathematics, a stationary study type was selected in the solver settings. This type of study analyzes the model in a time-independent manner.

Step 2: Create Geometry Object For the geometry of a 5 nm composite QD, a spherical radius of 2.5 nm was implemented. Within the 2.5 nm radius, a thickness layer of 1.5 nm for the shell was placed. The software demarcates the core to have a diameter of 2 nm and shell to have a thickness of 1.5 nm as shown in Figure 2.2 [54].

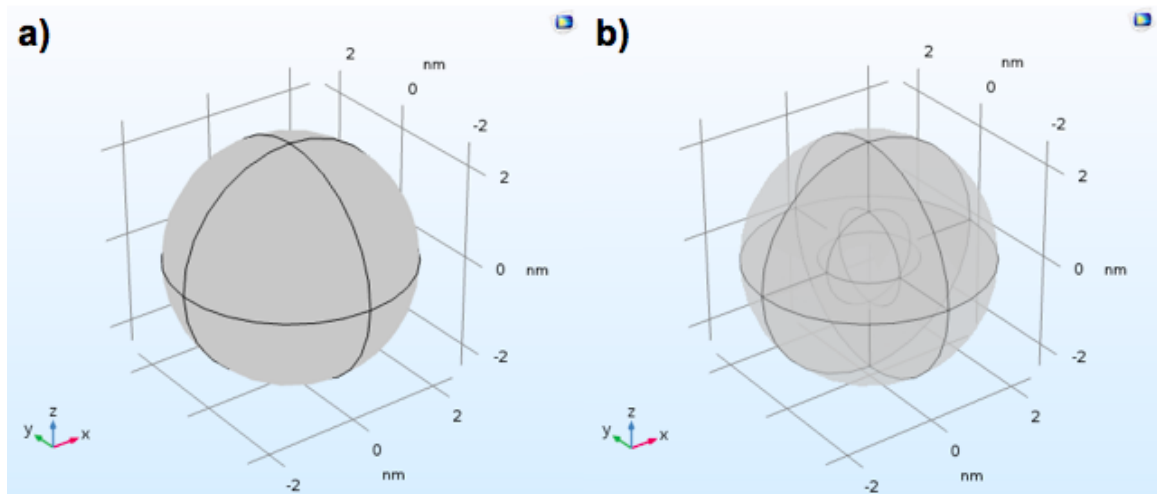


Figure 2.2: **Geometry of QD.** a) A 5 nm composite QD b) Within the composite QD, a core with a diameter of 2 nm, and a shell thickness of 1.5 nm were implemented.

Step 3: Specify Material Properties The equation-based modeling requires PDE in its coefficient form. Thus, the user inputs parameter values for a coefficient form PDE. The PDE was written as

$$\nabla \cdot (-c\nabla u - \alpha u + \gamma) + \beta \cdot \nabla u + au = d_a \lambda u. \quad (2.1)$$

By comparing this coefficient form PDE to the Schrödinger equation as shown in equation (1.3), α , β , and γ terms resulted to be zero coefficients, reducing equation (2.1) into

$$-c\nabla^2 u + au = d_a \lambda u, \quad (2.2)$$

where the non-zero coefficients of equation (2.2) are $c = \frac{\hbar^2}{2m}$, $a = V$, $d_a = 1$, $\lambda = E$, and $u = \psi$. By substituting these terms, we obtain back equation (1.3).

Moreover, additional parameters of CdSe/ZnS shown as a list of variables in Table 2.1 will provide with the numerical values needed for the coefficients. The needed values are the mass of the electron, Planck's constant, and built-in potential barriers of the semiconductor materials (both CdSe and ZnS). With these values, coefficient values such as the effective mass of the electron, effective mass of the hole, and coefficient terms of both electron and hole for CdSe, and ZnS were obtained.

Name	Expression	Value	Description
m	$me_const[1/kg]/e_const[1/C]$	5.6856E-12	Electron mass [$\frac{eV}{c^2}$]
\hbar	$hbar_const[1/(J \cdot s)]/e_const[1/C]$	6.5821E-16	Reduced Planck's constant [$eV \cdot s$]
m_e^*	0.13 m	7.3913E-13	Effective mass of electron [$\frac{eV}{c^2}$] [63]
m_h^*	0.4 m	2.2743E-12	Effective mass of hole [$\frac{eV}{c^2}$] [63]
V_CdSe	0	0	Built-in Potential barrier, CdSe [eV][25]
V_ZnS	0.9	0.9	Built-in Potential barrier, ZnS [eV][25]
c.e_CdSe	$\frac{\hbar^2}{2 \cdot 0.15 \cdot m_e^*}$	2.54E-19	c_e coefficient, CdSe
c.h_CdSe	$\frac{\hbar^2}{2 \cdot 0.45 \cdot m_h^*}$	8.4666E-20	c_h coefficient, CdSe
c.e_ZnS	$\frac{\hbar^2}{2 \cdot 0.25 \cdot m_e^*}$	1.524E-19	c_e coefficient, ZnS
c.h_ZnS	$\frac{\hbar^2}{2 \cdot 0.59 \cdot m_h^*}$	6.4576E-20	c_h coefficient, ZnS

Table 2.1: **Simulation Parameters.** Parameters used in the COMSOL Multiphysics 5.3. These are the parameters for CdSe/ZnS QD used in the coefficient form PDE [11].

Step 4: Define Physics Boundary Conditions After having created the geometry of the object, Dirichlet boundary conditions were placed at the boundaries of the surface of the composite QD as shown in Figure 2.3. These boundary conditions constrain the solutions of the PDE to be within the QD. To optimize the value of the solutions, FEM, was applied.

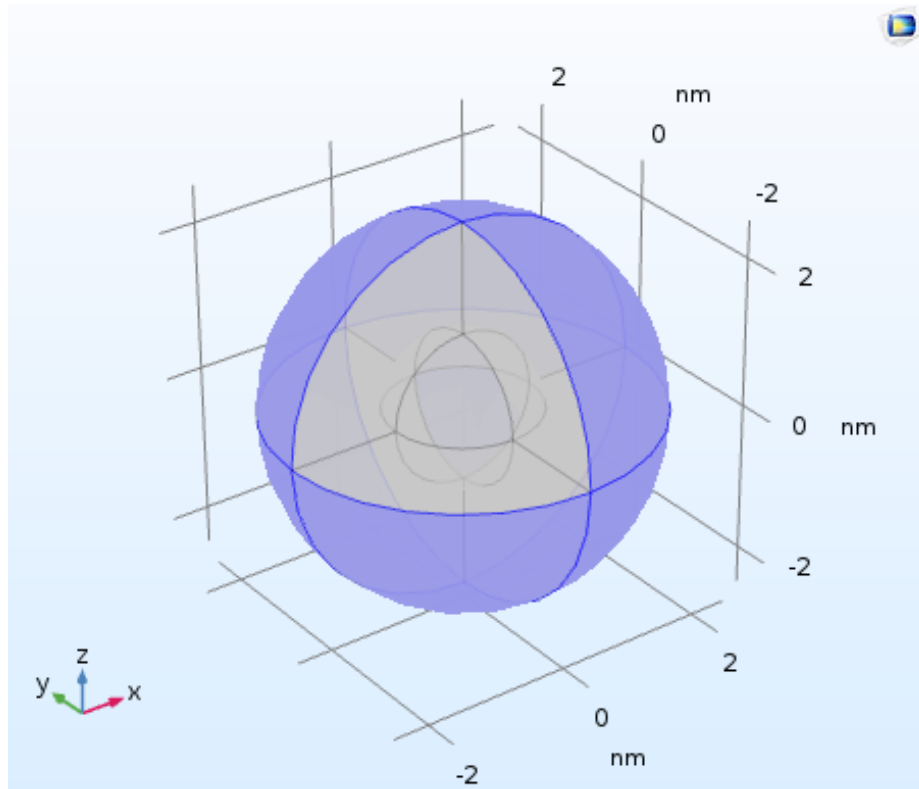


Figure 2.3: **Dirichlet Boundary Conditions on QD.** The boundary conditions cover the QD in blue, which ensure that solutions will be sought for within the confines of this boundary only.

Step 5: Create the Mesh For the mesh, FEM is used to divide the model into elements of geometrically simple shapes [1]. The use of different mesh size elements can vary the accuracy of the result, where refining the mesh will result in greater computational time and memory usage. The available mesh in our simulation were: extra course, course, normal, fine, finer, and extra fine. We were limited up to “finer” element sizes. The resulting mesh composed of tetrahedrons is shown in Figure 2.4.

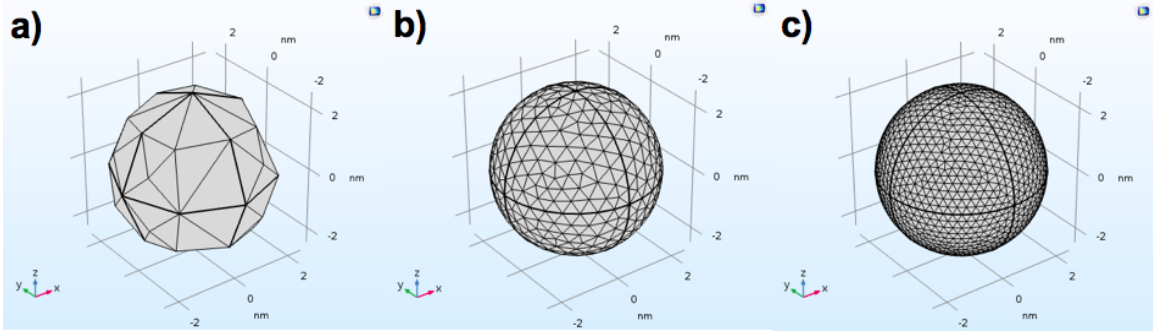


Figure 2.4: **Composite QD with FEM.** Using FEM, the size of the elements provided by COMSOL varied. Smaller elements for FEM, providing more exact numerical solution of the energy eigenvalues. (a) Extra coarse mesh (b) Normal mesh (c) Finer mesh.

Step 6: Run Simulation The simulation demonstrates the resulting energy eigenvalues of the study. Moreover, the simulation also provides with the probability density of the confined particle (Figure 2.5).

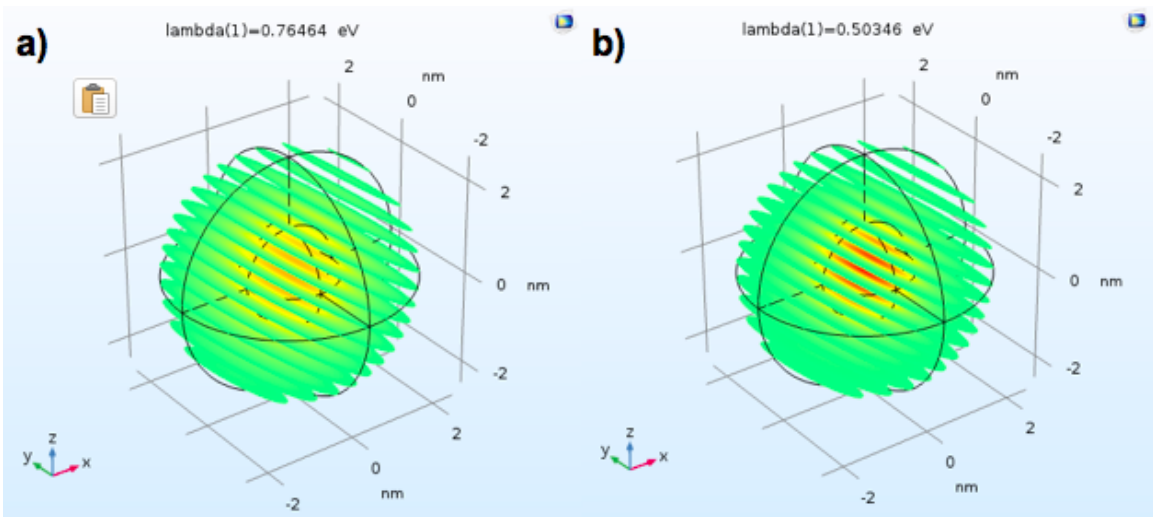


Figure 2.5: **Probability Density in COMSOL Multiphysics 5.3.** Regions of red indicate the highest likelihood of finding the particle. a) Electron confined in a QD well in its lowest energy eigenvalue b) Hole confined in a QD well in its lowest energy eigenvalue.

Step 7: Postprocess Results The resulting energy eigenvalues from this simulation were utilized to calculate the energy difference of the QD. The lowest energy eigenvalues from the electron and hole were used for the energy difference calculation as mentioned in chapter 1, section 1.4.3.

2.1.2 Statistical Methods

Error Analysis for Computational Results

The error analysis for our computational results followed the Newton-Raphson Method [7]. For the expected solution of the PDE, an approximate solution with associated error tolerance was given. The error observed in computational simulations was due to simplification of the mathematics in the algorithm, and round-off errors from finite numbers [42].

Chapter 3

Experimental Methods (Spectroscopy)

The experimental part of this investigation consists of the use of spectroscopy to test whether macromolecules produced from cells alter the opto-electronic properties of QDs. The results of this chapter will provide further experimentation for our computational model QD shown in chapter 2.

3.0.1 Materials

Spectroscopic Equipment

The spectroscopic equipment consisted of the following: UV LED (3.2 V, 20 mA) with a wavelength from 395 nm to 405 nm (2760014 RadioShack), UV/VIS optical fiber cable with a numerical aperture (NA) 0.22 consisting of acceptance angle of 12.7° (655307 Ocean Optics), sample cuvette, spectrometer (USB 650 Ocean Optics), and computer with OceanView 1.6.5 software. The experimental set up is shown in Figure 3.1.

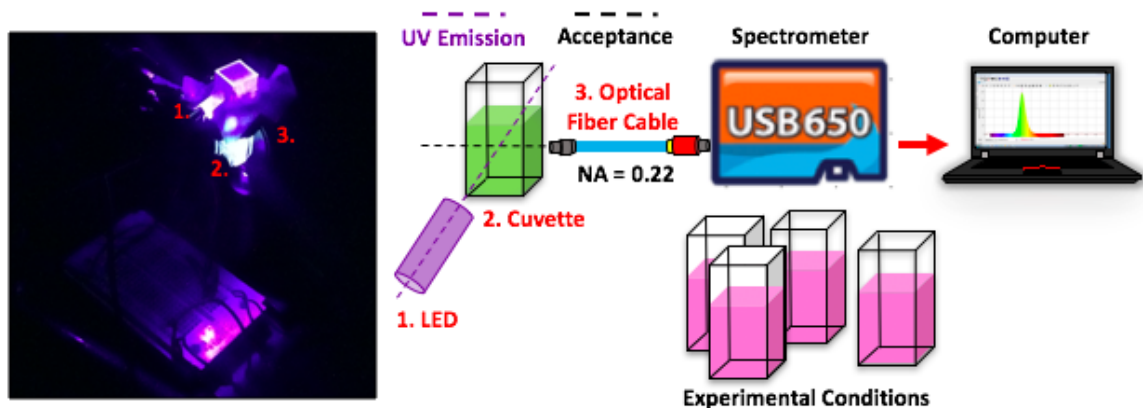


Figure 3.1: **Spectroscopic Equipment.** The colloidal sample of CdSe/ZnS QD was illuminated with a source of UV light at a temperature of 22.1°C. The sample fluorescence was collected by the optical fiber and directed to the spectrometer, where it was analyzed.

The distance of the optical fiber cable to the colloidal sample had been adjusted to provide with the most collection of light. Thus, the LED and the optical fiber cable were aligned orthogonal to each other so that the collection of light would not be saturated with UV light. In the spectrometer, the collected light passed through a diffraction grating splitting photons by wavelength. These photons traveled through the detector, striking its individual pixels and converting them into electrical signals. The signals were analyzed in the computer using OceanView 1.6.5 software to generate a spectra of intensity in arbitrary light units (a.u.) vs. wavelength (nm). For the software set up, the boxcar width averages spectral data and integration time allows more photons to be collected by the detector at a frame of time. The boxcar width and integration time could have been increased to raise the signal to noise ratio [2], but these were kept at default due to slow response of the computer. Thus, the set up was limited to the default settings: for boxcar width, 0; for integration time, 100 ms.

Chemical Materials

To analyze the interaction of QDs with various cells in spectroscopy, colloidal solutions of QDs were made using powder forms of CdSe/ZnS QDs. Due to their long term usage in terms of handling and storage, powder form QDs were obtained from manufacturers. For short term and immediate use, solubilized QDs were purchased from manufacturers. Details of the chemical experiments are found in the appendix D.

Hydrophobic CdSe/ZnS QDs Powdered form CdSe/ZnS QDs with hydrophobic surface reactants (748056 Sigma Aldrich) were dissolved in toluene (UN1294 Fisher Chemical), a non-polar solvent. This type of QDs served as a control variable to check their response in a cellular environment.

Hydrophilic CdSe/ZnS QDs Powdered and solubilized forms of CdSe/ZnS QDs with hydrophilic surface reactants (QSH-540-04 Ocean NanoTech, LLC), and (900244-250UL Sigma Aldrich), respectively, were used. These QDs were enabled to be biocompatible by the manufacturers, using polyethylene glycol (PEG), an inert polymer which does not interfere with the optical properties of the QD [60]. These commercially available forms of biocompatible CdSe/ZnS QDs have been well characterized in terms of their effects on biological cells as well [43].

Hydrogen Peroxide (H_2O_2) Hydrogen Peroxide, H_2O_2 (516813-500ML Sigma Aldrich), has been utilized. Because its by-products interacts with water molecules reactive oxygen species, ROS, are produced. These are the same macromolecules produced by cells. Using varying concentration of H_2O_2 , we can mimic what cells are doing to the QDs.

Chemotherapeutic Drugs To address our hypothesis, whether bioactive molecules and/or molecules from biological cells can alter the opto-electronic properties of QDs, we used chemotherapeutic drugs Anthracyclines [26] such as Doxorubicin, Dox, (4458 Sigma) and Daunorubicin, Dauno, (D8809 Sigma) as bioactive molecules. These anti-cancer drugs used to treat leukemic cancer cells have been studied in the Translation Biomedical Research Lab in terms of their possible prometastatic effects [56], and were used to also induce controlled changes in cellular activities leading to the production of charged molecules that might perturb the opto-electronic properties of QDs.

Dox is a well known bioreductive drug that undergoes a single electron reduction in solution, forms unstable semiquinone radical and promotes production of ROS in cells [41]. Thus, Dox in soluble medium, by itself, should produce bioactive molecules that might alter the photophysical properties of QD. Furthermore, owing to its widespread use, Dox has been conjugated with QDs so as to enhance its delivery in cells as part of the burgeoning Nano-Particle Mediated Drug Delivery (NPDD) research frontier [20] [22] [72]. Dauno, with similar usage as Dox, also produces bioactive molecules and promotes ROS production in cells with interesting differences compared to Dox [69]. These drugs enable us to induce ROS production in cancer cell lines and therefore such measurements assess the opto-electronic modulation of QD properties, if any. We now present the cells used in the study.

Biological Materials

HL60 Cells HL60 cells, which are a cell line derived from an acute myeloid leukemia patient, are non-adherent cells and grow in suspension [56]. These cells differentiate into neutrophil, monocyte, and macrophage lineages. Neutrophils and monocytes circulate through the blood and extravasate into tissues to carry out important antimicrobial activities at infected sites via chemical signals [29]. Monocytes become

macrophages once they enter the tissue [29]. These cells were purchased from HL-60 (ATCC[®] CCL-240[™]), cultured, and kept in an incubator at a temperature of 37°C and 5% CO₂. These cells were cultured with RPMI 1640 (11875093 Life Technologies), supplemented with 10% fetal bovine serum (FBS) and 1% Penicillin/Streptomycin as the growth medium [56]. Detailed culturing methods are found in appendix C. Since the NPDD already uses QDs with Dox and Dauno, we focused on cells that are the common targets of these Dox and Dauno. HL60 cells are excellent models of myeloid leukemic cells [24]. To model erythroid leukemia (where Dox and Dauno are also used), K562 cells were utilized. [52]

K562 Cells K562 cells are malignant multipotent, hematopoietic cells that spontaneously differentiate into progenitors of the erythrocytic, granulocytic and monocytic lineages. These cells are also non-adherent and grow in suspension. Similar to the culture method of HL60 cells [56], these cells were purchased from K-562 (ATCC[®] CCL-243[™]), cultured, and kept in an incubator at a temperature of 37°C and 5% CO₂. These cells were cultured with RPMI 1640 (11875093 Life Technologies), supplemented with 10% fetal bovine serum (FBS) and 1% Penicillin/Streptomycin as the growth medium. Detailed culturing methods are found in appendix C.

T98G Cells T98G cells model glioblastoma multiforme, a very aggressive form of brain cancer [53][45]. Glioblastoma multiforme is also the most common form of malignant primary tumor and there is yet no cure for it [53]. Because T98G cells are also adherent cells, the culture method differed from the case for HL60 and K562. However, these cells possess the same growth phases (lag-phase, log-phase and plateau phase) as HL60 and K562 [9]. Additional, steps included the use of Ca⁺⁺/Mg⁺⁺ free Dulbecco's phosphate-buffered saline (D-PBS) and 2.0 - 3.0 mL of Trypsin-EDTA solution. The former was used to rinse out traces of serum, which are considered to be Trypsin inhibitors, and the latter was used for the actual detachment

of cells [8]. We purchase T98G cells from T98G [T98-G] (ATCC[®] CRL-1690[™]), cultured, and kept in an incubator at a temperature of 37°C and 5% CO₂. Detailed culturing methods are found in appendix C. With T98G cells, we investigate the role of radiotherapeutically induced changes in cellular activities on the photophysical properties of QDs. As potential radiosensitizers (agents that enhance therapeutic outcome) [38], QDs' interactions with radiation induced ROS production in cells need to be examined.

Radiotherapeutic Materials

In addition to chemotherapy that is being employed to cells to induce controlled changes in cellular activities, radiotherapy is used as a second method to induce these control changes. For radiotherapy, Faxitron CellRad (160920-RH3 Faxitron), a compact, safe cabinet X-Ray unit was used to apply clinically lethal and sub-lethal doses of X-Ray to cells, where these doses induce ROS production in cells. In the context of this research, QDs become relevant as they are known to be radiosensitizers to enhance radiotherapeutic outcome [68].

3.0.2 Methods

QD Spectroscopy with Bioactive Molecules

QD spectroscopy (Figure 3.1) was carried out to test the effect of bioactive molecules on the opto-electronic properties of QDs. To prove the reliability of our setup, H_2O_2 , known to induce concentration-dependent reduction of fluorescence intensity in QDs as well as optical quenching was used on both hydrophobic and hydrophilic QDs [31] [47]. As shown in Table 3.1, concentrations of the H_2O_2 spanned three orders of magnitude: 0, 0.1, 1, 5 and 10%.

Experiment	Cell Line	Controlled Changes
Hydrophobic CdSe/ZnS QD (Control)	N.A.	Hydrophobic CdSe/ZnS QD with an emission peak at 540 ± 10 nm
Hydrophilic CdSe/ZnS QD (Control)	N.A.	Hydrophilic CdSe/ZnS QD with an emission peak at 540 ± 10 nm
H_2O_2	N.A.	Concentrations of 0%, 0.1%, 1%, 5%, 10%
Chemotherapy and Medium	N.A.	Chemotherapeutic drugs: Dauno and Dox
Chemotherapy	HL60	Chemotherapeutic drugs: Dauno and Dox
Chemotherapy	K562	Chemotherapeutic drugs: Dauno and Dox
Radiotherapy	HL60	20 Gy X-Ray. Measurement done 1 hr post-radiotherapy
Radiotherapy	K562	20 Gy X-Ray. Measurement done 1 hr post-radiotherapy
Radiotherapy	T98G	20 Gy X-Ray. Measurement done 1 hr post-radiotherapy

Table 3.1: **Experimental Conditions.** Nine experiment conditions along with their descriptions. The first two experimental conditions serve as control variables, and the rest of the experimental conditions had CdSe/ZnS QDs introduced after the controlled changes.

To unveil any photophysical changes in QD spectra by bioactive molecules, QD spectroscopy was done using Dox (5 μM) and Dauno (1 μM) in complete cell culture medium without cells. The detailed steps in getting the concentrations, duration of QD in media prior to measurements are presented in appendix D.

In order to quantify the changes induced in the opto-electronic properties of QDs by charged ions of cellular origin, Dox and Dauno-treated HL60 and K562 cells were used. The final concentrations of Dox and Dauno were maintained at 5 μM and 1 μM , respectively (as in the culture-medium-only cells above). This enabled the comparison of changes induced only by Dox and Dauno without cells with changes induced by Dox and Dauno with cells. All experiments were carried out in triplicates as N1, N2, and N3. Each of these triplicate experiments involved 5 acquisitions of spectra. Details are given in appendix D and the outcome of the conditions are tabulated in Table 4.3.

Lastly, to provide a basis for confirmation and for mechanistic insights, another known way in which cellular activities are changed leading to production of ROS, namely, radiotherapy, was applied for spectroscopy. Using Faxitron CellRad, HL60, K562, and T98G cells were irradiated with 20 Gy X-Ray. All experiments were carried out in triplicate as well. Table 4.3 summarizes the outcome of the conditions and appendix D provides the exact protocols employed.

3.0.3 Statistical Methods

Error Analysis Experimental Results (Emission Wavelength)

Using Origin Analysis Software (OriginLab 2017), nonlinear curve fits were made onto average intensity in arbitrary light units (a.u.) vs. wavelength (nm) plots indicated as a) in chapter 4: these plots were averaged from 5 trials of intensity in arbitrary light units (a.u.) vs. wavelength (nm) plots of an experimental condition. Since emission peaks were from the fluorescence generated by the colloidal QDs, Gaussian functions were fitted onto the plots [25]. The Gaussian fit utilized the Levenberg Marquardt iteration algorithm, which was limited to 400 iterations. If the limit were not reached, the iterations underwent until the fit had converged with a chi-squared tolerance of 1×10^{-7} . Once the Gaussian fit had been made, the mean and standard deviation of the emission peak were found. We use the standard deviation, σ , to calculate for the standard error of the mean (SE) using equation (3.1):

$$SE = \frac{\sigma}{\sqrt{N}}, \quad (3.1)$$

where N is the number of trials. Thus, an expected emission value is obtain in the form of $m \pm SE$ allowing for it to be used to compare with the manufacturers' values and computational results. For comparing values among different experimental conditions, statistical comparison of experimental results was done using Analysis of Variance, ANOVA, from OriginLab 2017.

Statistical Comparison using ANOVA

The use of ANOVA is due to reliability in statistical comparison of multiple data sets [40]. Thus, emission peaks among different experimental conditions were done by first plotting 5 different trials of each experimental condition. Then Gaussian fits were again used for each trial in order to determine the peaks of the emissions

[25]. In ANOVA, one-way ANOVA was used to test different significance levels with p-values of 0.05, 0.01, 0.001, and 0.0001, which are indicated as *, **, ***, and ****, respectively. The smaller the p-value, the greater the difference is between the control and experimental condition. The means comparison test given by the software was used to create box charts in peak intensity in arbitrary light units (a.u.) vs. condition. These are indicated as b) in the Figures of chapter 4.

Chapter 4

Results

The results of the energy eigenvalues of the Schrödinger equation from CdSe/ZnS QDs are presented in this chapter, serving as a basis for further modeling. The experimental spectroscopic results are also presented in this chapter. Spectroscopic measurements and analysis of optically excited colloidal CdSe/ZnS QDs with HL60, K562, and T98G cell lines were performed following chemotherapy and radiotherapy.

4.1 Computational Results

We simulated the four lowest energy eigenvalues of the electron and hole separately using Schrödinger equation with the finer mesh. These energy eigenvalues are shown in tables 4.1 and 4.2. For the simulation of the electron, the number of iterations was 13 with an estimated error of 7.4×10^{-7} eV. This simulation computed for 16 seconds using a physical and virtual memory of 1.45 GB and 1.64 GB. For the simulation of the hole, the number of iterations was 11 with an estimated error of 0.94×10^{-7} eV. This simulation computed for 15 seconds using a physical and virtual memory of 1.35 GB and 1.49 GB. One can follow the simulation log for this simulation in appendix E. We use their first energy levels along with the energy band gap of CdSe (1.74 eV [12]), and coulombic potential terms to calculate for ΔE in equation 1.11. With these

Energy Level, n	Energy Eigenvalue (eV)
1	$0.76 \pm 7.4 \times 10^{-7}$
2	$1.35 \pm 7.4 \times 10^{-7}$
3	$1.35 \pm 7.4 \times 10^{-7}$
4	$1.35 \pm 7.4 \times 10^{-7}$

Table 4.1: **Energy Eigenvalues of the Electron in CdSe/ZnS QD Well.** The four lowest energy eigenvalues of the electron were obtained from CdSe/ZnS that has a core diameter of 2 nm, and shell thickness of 1.5 nm.

Energy Level, n	Energy Eigenvalue (eV)
1	$0.50 \pm 3.7 \times 10^{-7}$
2	$0.94 \pm 3.7 \times 10^{-7}$
3	$0.94 \pm 3.7 \times 10^{-7}$
4	$0.94 \pm 3.7 \times 10^{-7}$

Table 4.2: **Energy Eigenvalues of the Hole in CdSe/ZnS QD Well.** The four lowest energy eigenvalues of the hole were obtained from CdSe/ZnS that has a core diameter of 2 nm, and shell thickness of 1.5 nm.

energy eigenvalues, we calculate the emission of CdSe/ZnS used in our spectroscopic experiment.

4.2 Spectroscopic Results

4.2.1 Hydrophobic and Hydrophilic QDs Alone

Following Table 3.1, we plotted an intensity in arbitrary light units (a.u.) vs. wavelength (nm) plot of the hydrophobic QD as shown in Figure 4.1. We found its emission peak at $550 \text{ nm} \pm 30$, which is within the expected value of $540 \pm 10 \text{ nm}$ provided by the manufacturer [6]. Likewise, we plotted an intensity in arbitrary light units (a.u.) vs. wavelength (nm) plot of the hydrophilic QD as shown in Figure 4.2. We found its peak emission was at $539 \pm 30 \text{ nm}$, which is within the expected value

of 540 ± 10 nm provided by the manufacturer [6]. These spectroscopic results, using only QDs, confirm our set-up does work and yields expected fluorescent spectra.

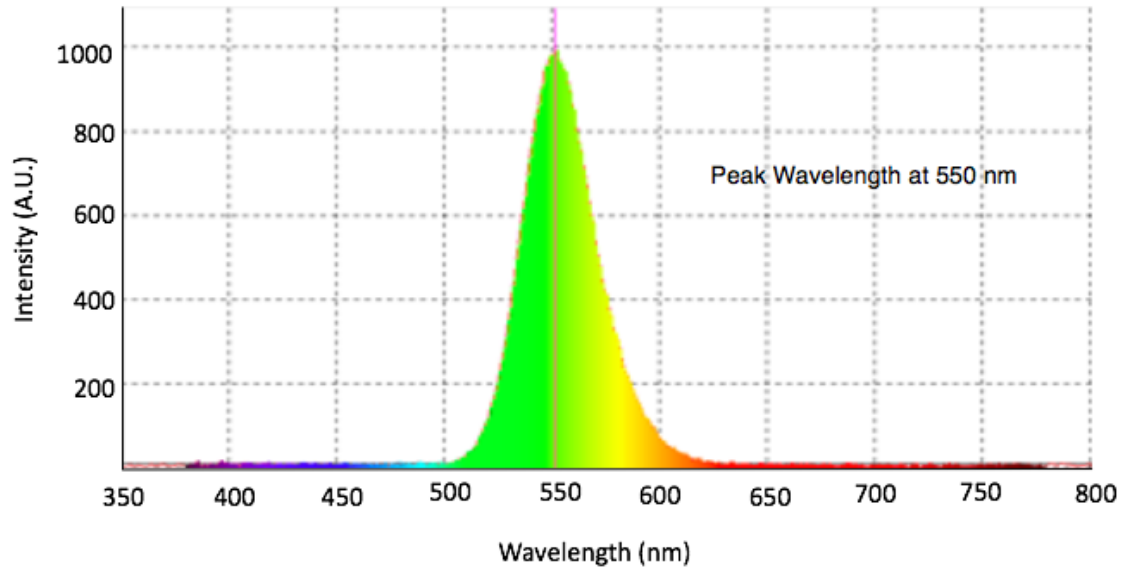


Figure 4.1: **Hydrophobic CdSe/ZnS QD Spectra.** From this intensity in arbitrary light units (a.u.) vs. wavelength (nm) plot, the peak emission locates at 550 nm.

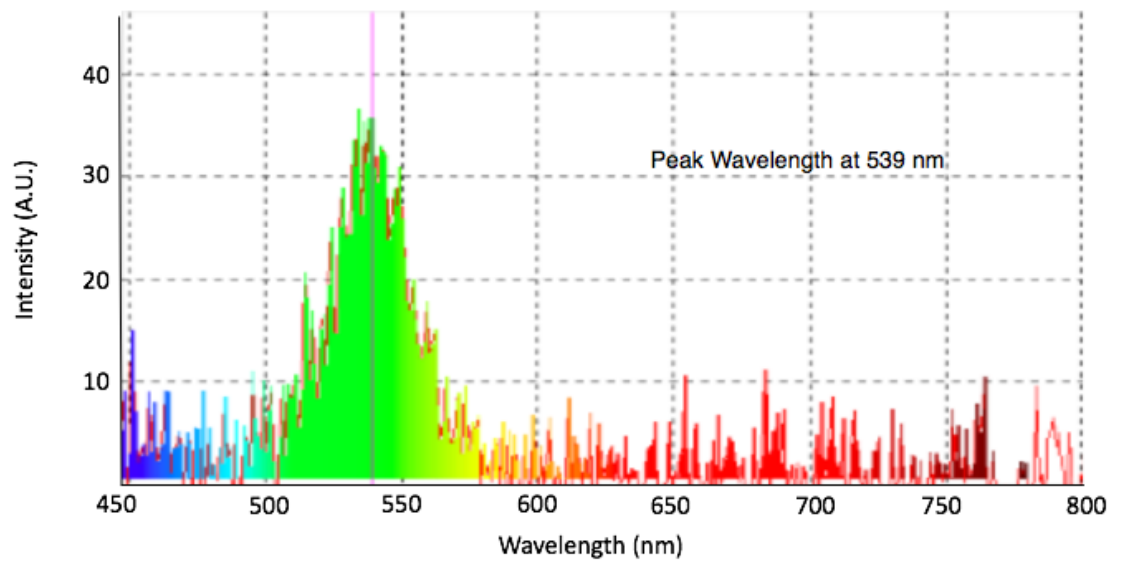


Figure 4.2: **Hydrophilic CdSe/ZnS QD Spectra.** From this intensity (a.u.) vs. wavelength (nm) plot, the peak emission locates at 539 nm.

4.2.2 Hydrophobic and Hydrophilic QDs with Hydrogen Peroxide

In Figures 4.3 and 4.4, increasing concentrations of hydrogen peroxide, H_2O_2 , decrease the intensity of QDs, leading to optical quenching. These experiments of Hydrophobic and Hydrophilic QDs with H_2O_2 lead to a first step basis confirmation to investigate the bioactive molecules produced by cells [31] [23] [47].

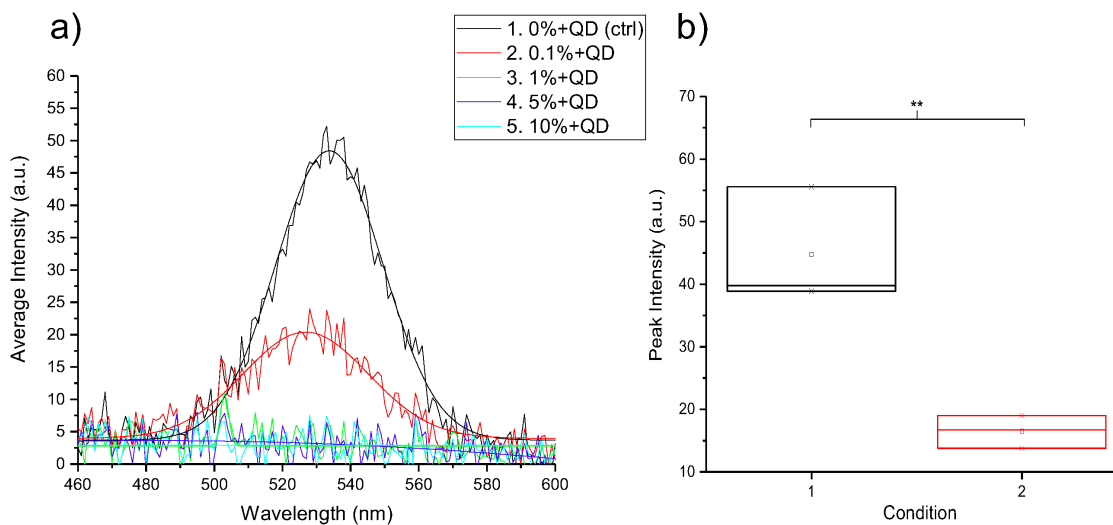


Figure 4.3: **Spectra and Statistical Comparison for Hydrophobic CdSe/ZnS QD with H_2O_2 .** a) The intensity modulated with varying concentrations of H_2O_2 when compared with control (condition 1). b) Condition 1 and 2 showed statistically significant difference ($p < 0.01$ or **).

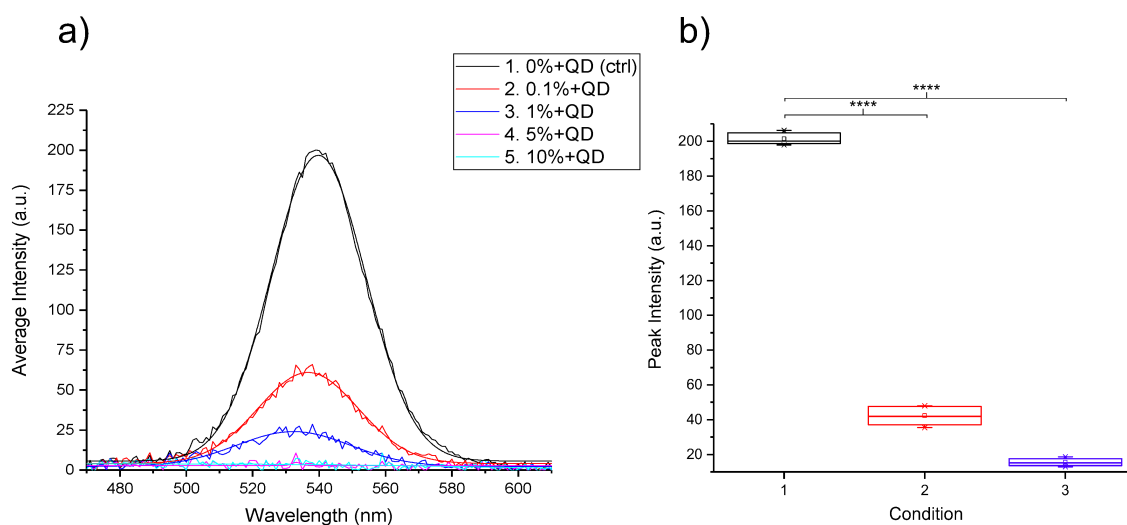


Figure 4.4: **Spectra and Statistical Comparison for Hydrophilic CdSe/ZnS QD with H_2O_2 .** a) The intensities also modulated with varying concentrations of H_2O_2 when compared with condition 1. b) Condition 2 and 3 showed statistically significant differences ($p < 0.0001$ or ****) when compared with condition 1.

4.2.3 Hydrophilic QDs with Bioactive Molecules and Cells

With the addition of chemotherapy drugs (dox and dauno) onto the medium with QDs, the intensity of the QDs modulated as shown in Figure 4.5, and had statistical significant differences ($p < 0.0001$).

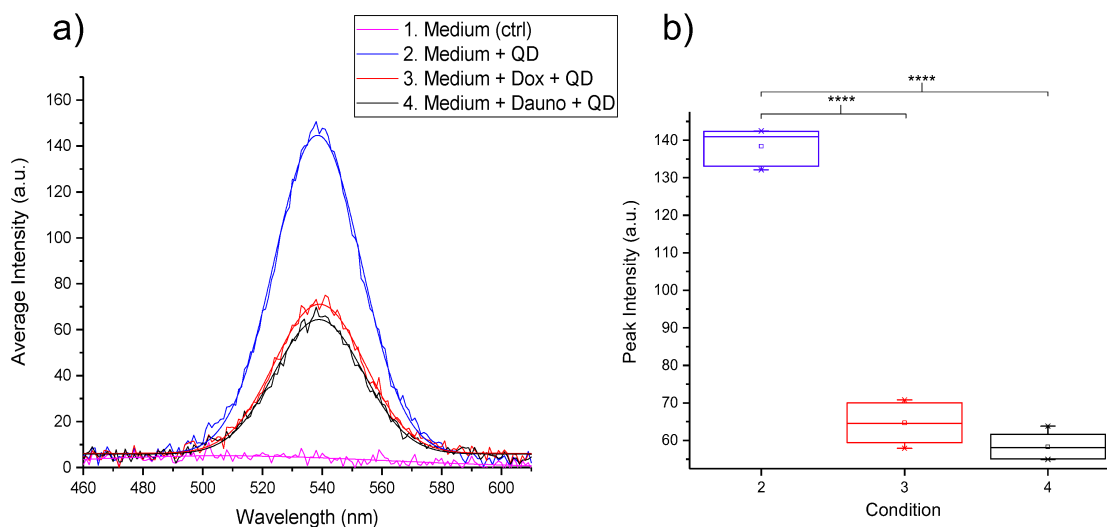


Figure 4.5: **Spectra and Statistical Comparison for Hydrophilic CdSe/ZnS QD with Medium and Chemotherapy Drugs.** a) The intensities of medium with chemotherapy drugs (conditions 3 and 4) decreased when compared with condition 2. b) Dox (condition 3) and Dauno (condition 4) treatments showed statistically significant differences ($p < 0.0001$ or ****) when compared with control (condition 1).

Hydrophilic QDs with Cells Altered by Chemotherapy

For the case of hydrophilic QDs with HL60 cells, significant changes in intensity were observed as shown in Figure 4.6. Statistically significant differences ($p < 0.0001$) were observed for Dox (condition 2), and Dauno (condition 3) treatments. Similarly, for the case of hydrophilic QDs with K562 cells, significant changes in intensity were observed showing the same statistically significant values as hydrophilic QDs with HL60 cells as shown in Figure 4.7.

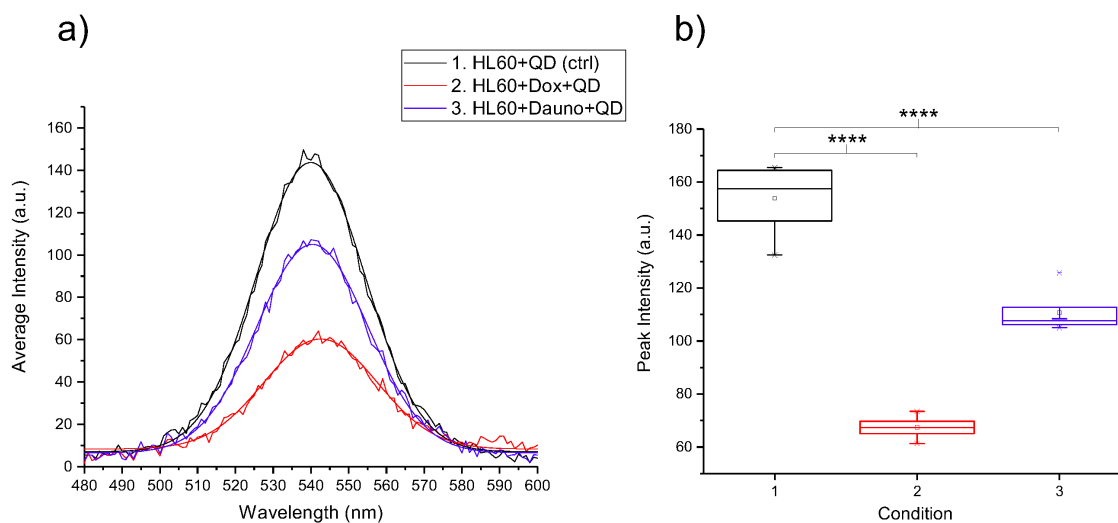


Figure 4.6: **Spectra and Statistical Comparison for HL60 Cells Treated with Chemotherapy Drugs.** a) The intensities decreased when compared with control (condition 1). b) Both Dox (condition 2) and Dauno (condition 3) treatments showed statistically significant differences ($p < 0.0001$ or ****) when compared with control (condition 1).

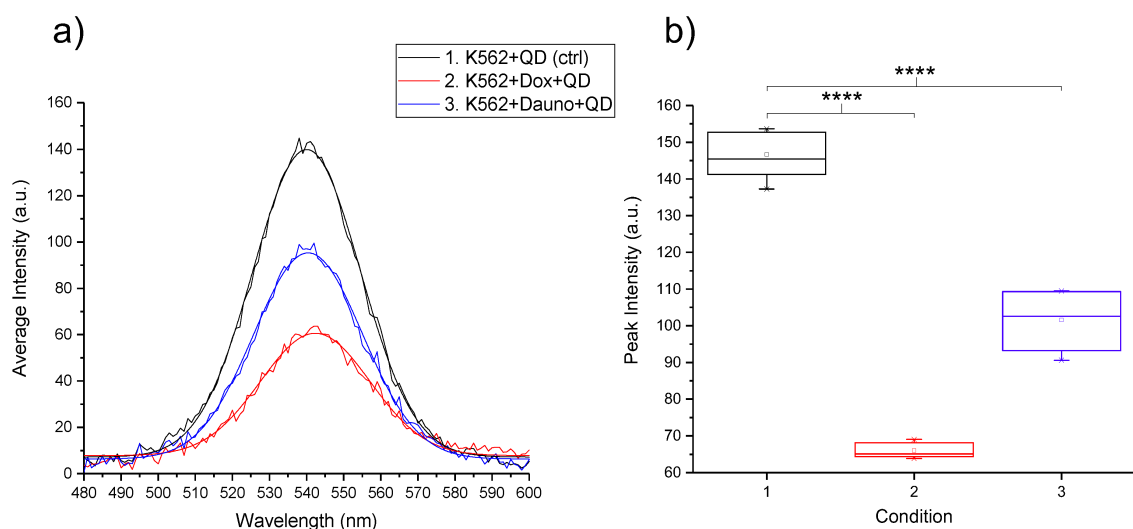


Figure 4.7: **Spectra and Statistical Comparison for K562 Cells Treated with Chemotherapy Drugs.** a) The intensities decreased when compared with the control (condition 1). b) Both Dox (condition 2) and Dauno (condition 3) treatments showed statistically significant differences ($p < 0.0001$ or ****) when compared with control (condition 1).

Hydrophilic QDs with Cells Altered by Radiotherapy

After the cells had been treated with 20 Gy X-rays of radiotherapy, QDs were introduced 1 hr after radiotherapy onto the sample. The emission spectra of the QDs due to the ROS produced by HL60 cells resulted with a statistically significant ($p < 0.001$) decrease in intensity as shown in Figure 4.8. Similarly, K562 examined 1 hr after 20 Gy X-rays of radiotherapy showed a statistically significant ($p < 0.0001$) decrease in intensity as shown in Figure 4.9. However, T98G cell lines examined 1 hr after 20 Gy X-rays radiotherapy showed fluctuating intensity. These differences were observed as N1, N2 and N3 experiments. For N1, quenching (statistically significant $p < 0.001$) was observed as shown in Figure 4.10. For N2, enhancement ($p < 0.01$) was observed as shown in Figure 4.11. For N3, no significant difference (NS) was observed as shown in Figure 4.12.

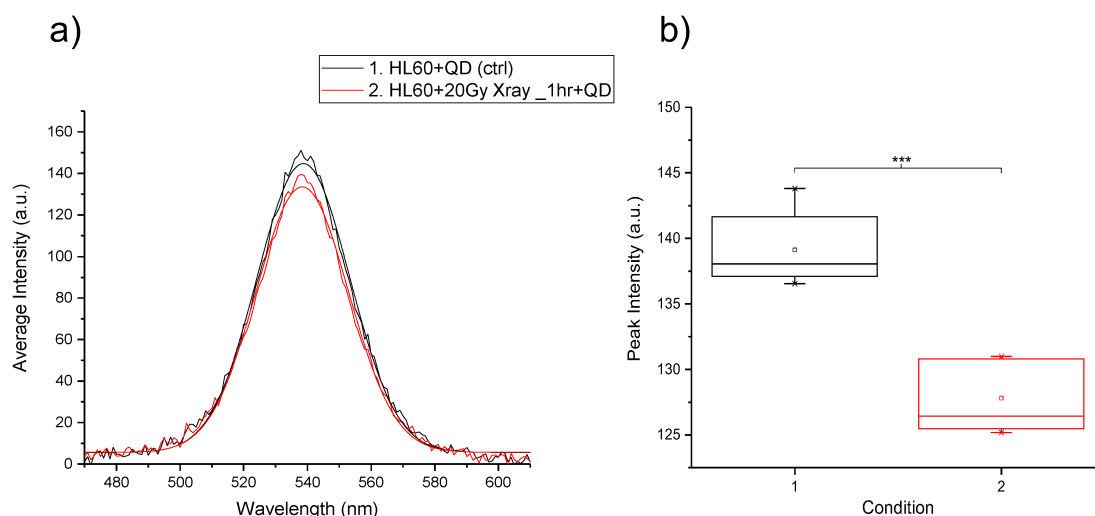


Figure 4.8: **Spectra and Statistical Comparison for HL60 Cells Treated with Radiotherapy.** a) The intensity decreased compared with control (condition 1). b) Condition 2 showed statistically significant difference ($p < 0.001$ or ***) when compared with control (condition 1), indicating quenching.

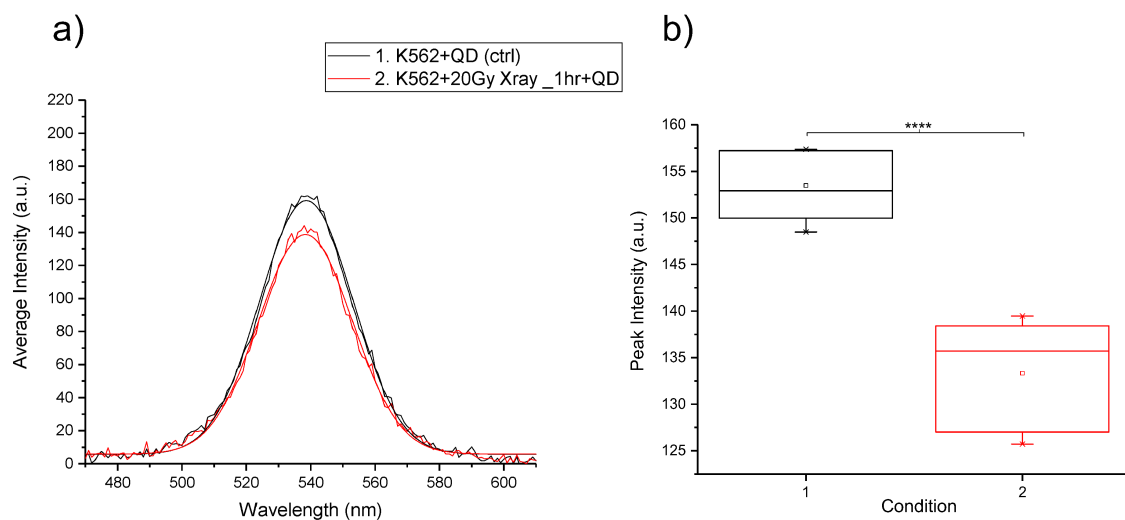


Figure 4.9: **Spectra and Statistical Comparison for K562 Cells Treated with Radiotherapy.** a) The intensity decreased compared with control (condition 1). b) From the statistical analysis, emissions showed statistically significant differences with $p < 0.0001$ (****) when compared with control (condition 1), indicating quenching.

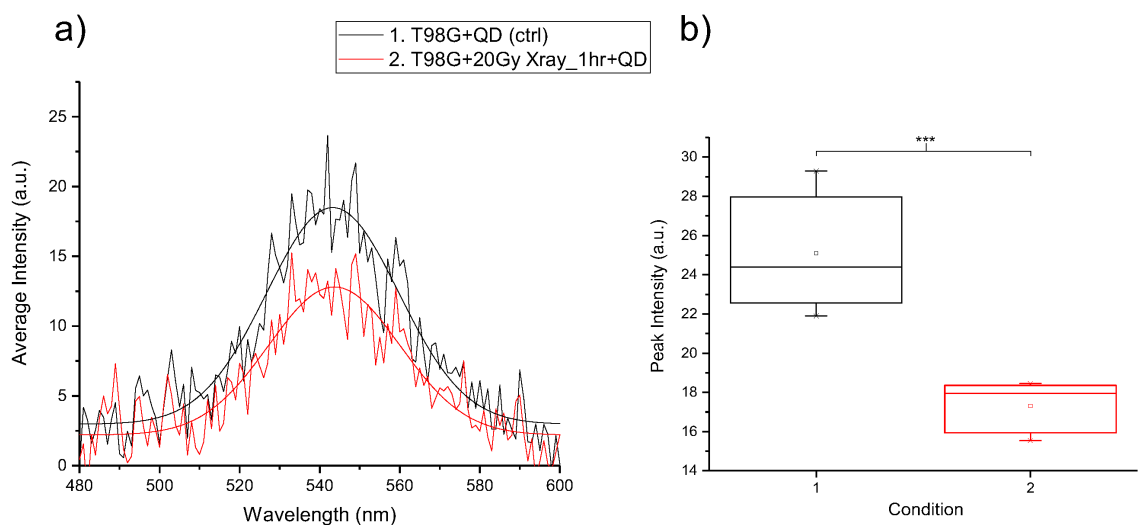


Figure 4.10: **Spectra and Statistical Comparison for T98G Cells Treated with Radiotherapy (N1).** a) The intensity decreased compared with control (condition 1) b) Emissions showed statistically significant difference ($p < 0.001$ or ***), indicating quenching.

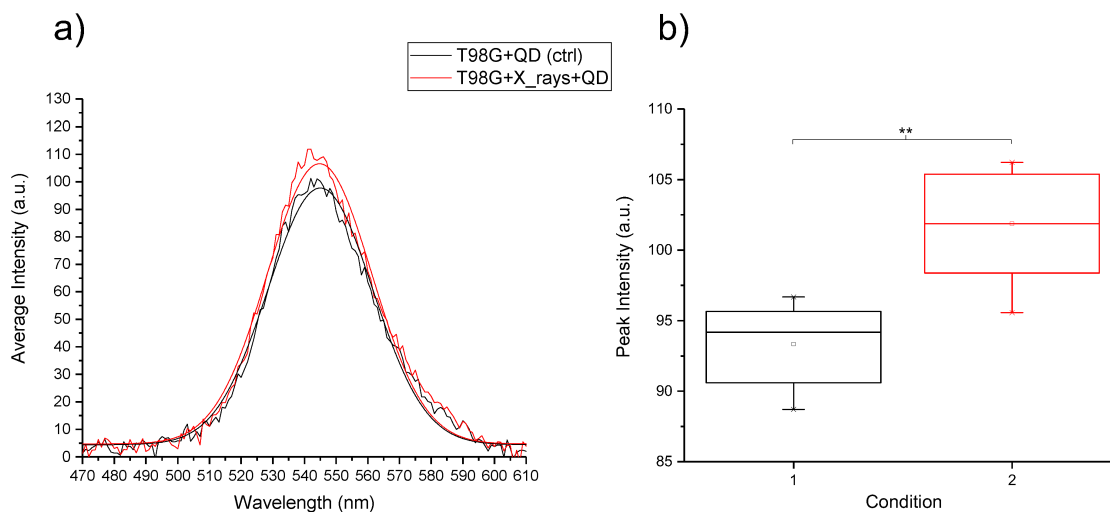


Figure 4.11: **Spectra and Statistical Comparison for T98G Cells Treated with Radiotherapy (N2).** a) From the average intensity (a.u.) vs. wavelength (nm) plot, the intensity increased. b) Emissions showed statistically significant difference ($p < 0.01$ or **) when compared with control (condition 1), indicating enhancement.

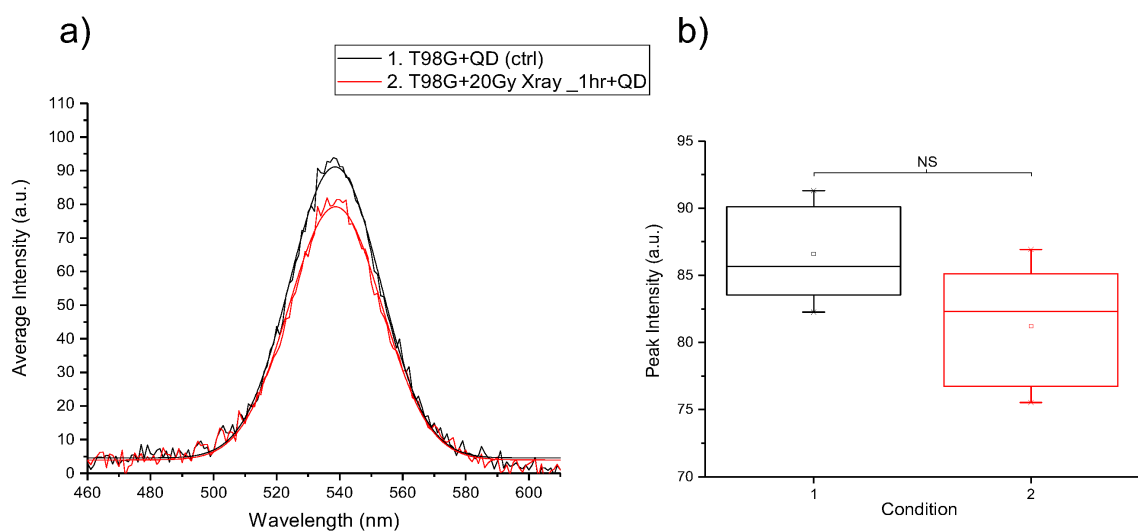


Figure 4.12: **Spectra and Statistical Comparison for T98G Cells Treated with Radiotherapy (N3)**. a) The intensity decreased compared with control (condition 1). b) Even with an intensity decrease, statistical comparison indicates that there was no significant (NS) difference between the conditions.

Experiment	Cell Line	Outcome
Hydrophobic CdSe/ZnS QD (Control)	N.A.	Emission at 550 ± 30 nm
Hydrophilic CdSe/ZnS QD (Control)	N.A.	Emission at 539 ± 30 nm
H_2O_2	N.A.	When QDs were present with H_2O_2 in a concentration dependent manner, ROS from H_2O_2 modulates QD intensity leading to optical quenching.
Chemotherapy and Medium	N.A.	Cells producing ROS cause intensity modulation (opto-electronic modulation) leading to optical quenching.
Chemotherapy	HL60	Cells producing ROS cause intensity modulation (opto-electronic modulation) leading to optical quenching.
Chemotherapy	K562	Cells producing ROS cause intensity modulation (opto-electronic modulation) leading to optical quenching.
Radiotherapy	HL60	Results show statistically significant decrease in average intensities for measurements done 1 hour after radiotherapy.
Radiotherapy	K562	Results show statistically significant decrease in average intensities for measurements done 1 hour after radiotherapy.
Radiotherapy	T98G	There was a quenching (N1), enhancement (N2) and no significant difference (N3) of the emission spectra of the colloidal dispersions due to the ROS produced by cells. These samples were examined 1 hour after radiotherapy.

Table 4.3: **Experimental Conditions Outcome.** Nine experimental conditions along with their outcomes. The first two conditions serve as controls, and the rest of the experimental conditions had CdSe/ZnS QDs introduced after cells had been treated with chemotherapy and radiotherapy.

Chapter 5

Discussion and Conclusions

5.1 Discussion

5.1.1 QD Opto-Electronic Properties Simulated in COMSOL Multiphysics

The FEM approach for solving the Schrödinger equation for QDs employed in this work yielded excellent agreement with experimental and manufacturer's values within the margins of error. Followed by equation 1.11, and using the first energy eigenvalues from Tables 4.1 and 4.2, ΔE yielded roughly 2.28 eV, which translates to an emission of 543.8 nm. Recent reports involving the successful use of this FEM approach exist [62] [37]. Moreover, our specific implementation of this FEM approach using COMSOL Multiphysics is also not novel [37] [35]. Hoang et al. used FEM in COMSOL Multiphysics for full-wave simulations of plasmonic nanopatch antennas coupled with QDs to study ultrafast spontaneous emission. Hartsfield et al., adopted FEM in COMSOL Multiphysics for enhancing light's coupling to a single QD with plasmonic cavities. Part of the novelty of this work lies in the focused investigation of possible changes in the opto-electronic properties of QDs due to bioactive molecules

and charged species of cellular origin. Alterations due to H_2O_2 , in view of those due to bioactive molecules from chemotherapeutic drugs are discussed next.

5.1.2 Fluorescence Intensity Modulation of QDs with Hydrogen Peroxide

The set of experiments involving both hydrophobic and hydrophilic QDs in the presence of various concentrations of hydrogen peroxide, H_2O_2 , produced expected results, namely, concentration-dependent modulation of fluorescent intensity, ending with optical quenching. This result has been reported for various nanocrystal QDs including CdSe/ZnS

[34] [10] [31]. Various mechanisms postulated to explain this intensity modulation and optical quenching include charge transfer and Förster Resonance Energy Transfer [10]. Since we have reproducibly obtained concentration-dependent intensity modulation, the setup and approach used in this work can enable further probing of the mechanism(s) of opto-electronic modulation of QDs by H_2O_2 and other reactive oxygen species (ROS). In general, the partial reduction of molecular oxygen leads to the generation of ROS, hence, many examples of ROS abound, including superoxide radical (O_2^-), hydroxyl radical (OH^-) and hypochlorous acid ($HClO$) [30]. It is therefore not surprising that radicals in chemotherapeutic drugs, even in the absence of cells, could lead to fluorescence intensity modulation. We discuss the experiments with bioactive molecules in Dox and Dauno in the next section.

5.1.3 Bioactive Molecules Alter Opto-Electronic Properties of QDs

The highly significant reduction in peak fluorescence intensity of QDs by 5 μ M Dox and 1 μ M Dauno, in the absence of cells, which we reported in chapter 4, section

4.2.3, is one of the major findings of this piece of research. This confirms one aspect of our hypothesis: bioactive molecules do alter the opto-electronic properties of QD. Dox has been conjugated with QDs to enhance the intracellular delivery of the the cancer drug [74]. But our result confirms the presence of bioreductive molecules in Dox, which alter the photophysical properties of the QDs. Hence, such alterations must be considered in the context of biomedical imaging, even in the estimation of uptake of the drug when such is based on QD fluorescence. Furthermore, Dox is already known to form an unstable semiquinone radical after a one-electron reduction in an aqueous environment, leading to the production of ROS [41]. Just as in our results, Dauno (1 μ M), which causes intensity modulation of QD fluorescence, is known to produce similar reductive effect in aqueous medium just as Dox [66]. A pertinent question that serves as a second future work engendered by the present result, is whether bioactive molecules can enhance, instead of merely reducing fluorescence intensity. Enhancement as well as reduction would then provide a better template for part of the ultimate goal of this work: opto-electronic modulation of QDs. Of course, the spectroscopic experiments involving QDs, Dox and Dauno and cells themselves, need to be discussed.

5.1.4 Molecules from Cells During Chemotherapy Modulate QD Fluorescence

The cellular environment is very complex. Various ROS are present in different competing amounts [19]. It must be emphasized that although ROS in cells and living organisms was discovered sixty years ago, their positive physiological roles, their cytotoxicity, and their mechanisms of actions are still issues of intensive debate and exploration [61] [57]. While open to new and increasing knowledge about cellular ROS, our experiments involved well-known increase in cellular ROS production due to chemotherapeutic drugs [41]. The highly significant reduction in fluorescence intensity

found when cells were treated with Dox and Dauno suggest that cells themselves do not reverse the result already obtained with the drugs in cell culture medium without cells. Since ROS is present in the Dox or Dauno-treated medium with or without cells, intensity modulation is expected, just as obtained in the results with chemotherapy treated HL60 and K562 cells. Furthermore, when blood cells are activated by agonists such as chemotherapeutic drugs, a dynamic homeostatic struggle ensues between intracellular ROS and extracellular ROS because cells themselves produce molecules capable of removing ROS such as super-oxide dismutase (SOD) [30] [32]. Thus, the apparent differences we find between the attenuation of fluorescence intensity of CdSe/ZnS by Dox/Dauno without cells and Dox/Dauno with cells suggests that cells produce molecules (such as SOD and ROS) that alter the photophysical properties of QD. Hence, we have results suggesting that the second aspect of the hypothesis in the work holds. This interpretation can be verified and it is now suggested as future experiment. SOD will be added to the chemotherapeutic experiments without cells. However, even in this work, further experiments were designed to confirm whether controlled changes in cells can modulate QD fluorescence. This was the essence of the radiotherapy experiments and the results obtained are discussed next.

5.1.5 Molecules from Cells Post-Radiotherapy Modulate QD Fluorescence

There is enhanced ROS production in irradiated cells [13] [65]. The enhanced ROS production is caused by radiolysis of water by ionizing radiation [16]. In fact, it is the increased ROS that contributes to cell-killing as these ROS can cause DNA lesions. Interestingly, some cells are much more radiosensitive than others [51]. Explicitly, blood cells and blood cell lines (e.g. HL60 and K562) are much more radiosensitive than neuronal or glial cells and cell lines (e.g., T98G). Part of the reason for differences in radiosensitivity is local availability of molecular oxygen. Such local oxygen

react with the DNA lesions caused by radiation-induced ROS to form stable DNA peroxides, reducing the prospects of DNA repair thereby leading to increased cell death. Therefore cancer cells that receive less or consume more oxygen (e.g. brain cancer cells) are usually less susceptible to radiotherapy than well oxygenated cancer cells consuming little oxygen (e.g. blood cancer cells). Obviously, we exploited these differences in the design of our radiotherapy experiments by choosing highly radiosensitive cells (HL60 and K562) and radioresistant cells (T98G).

The highly significant reduction in fluorescence intensity in the cases of HL60 and K562 is now easy to explain. Increased ROS production and the consumption of less oxygen in these blood cancer cells permits greater perturbation of the QDs by ROS complexes than in the case of T98G cells. No wonder the results with T98G cells also fluctuated, depending on the growth phase of the cells. The T98G cells were irradiated when the cells were rapidly growing and consuming more oxygen during the so-called log-phase (figure 4.10) and when growth had slowed down in the plateau phased (figure 4.12). Remarkably, cells that had been kept 2 days beyond plateau (no longer dividing and dying) even showed apparent enhanced fluorescence (Figure 4.11). These results might engender QD-based assays for testing cellular radiosensitivity in mixed cell or tissue environments.

5.1.6 Simulations of Possible Mechanisms

In order to set the stage for realizing some of the goals of this research, it should be possible to simulate the optical modulation of QD by bioactive molecules and molecules.

The possible mechanisms that explains the optical modulation are enlisted in the following manner:

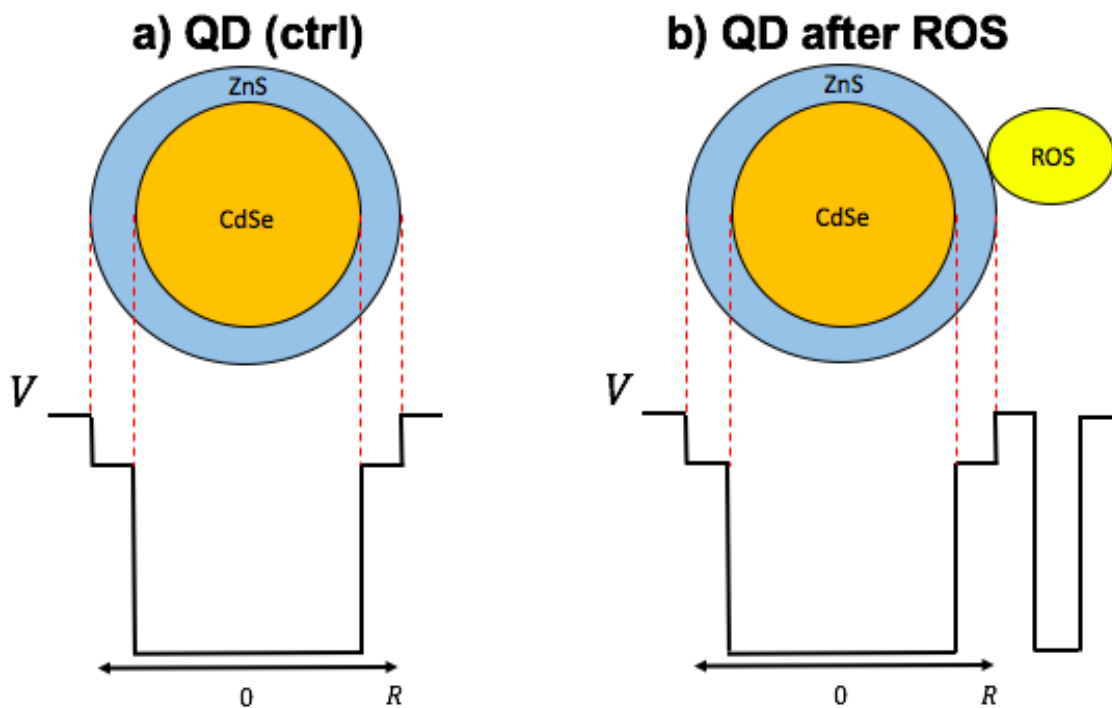


Figure 5.1: **First Possible Mechanism.** Bioactive molecules such as ROS attach themselves to the QD changing the original built-in potential well of the 1D finite CdSe/ZnS QD. Particles confined in the QD potential tunnel through into the built-in potential well created by ROS.

1. QDs form conjugates with bioactive molecules [46], making for excited electrons to be transferred onto bioactive molecule. This energy transfer (FRET) can be attributed to the change in the built-in potential of the system where electrons tunnel (Figure 5.1) [73] [36].
2. Bioactive molecules change the crystal structure of the QD, inducing a change in the electronic behavior and as a consequence its optical properties. Changes in the shell material property is shown in Figure 5.2. Changes in the core material property occurs when bioactive molecules diffuse through the shell material to reach to the QD's core [47] as shown in Figure 5.3 or even indicate defects of the QD, where the shell had not properly coated the core [25].

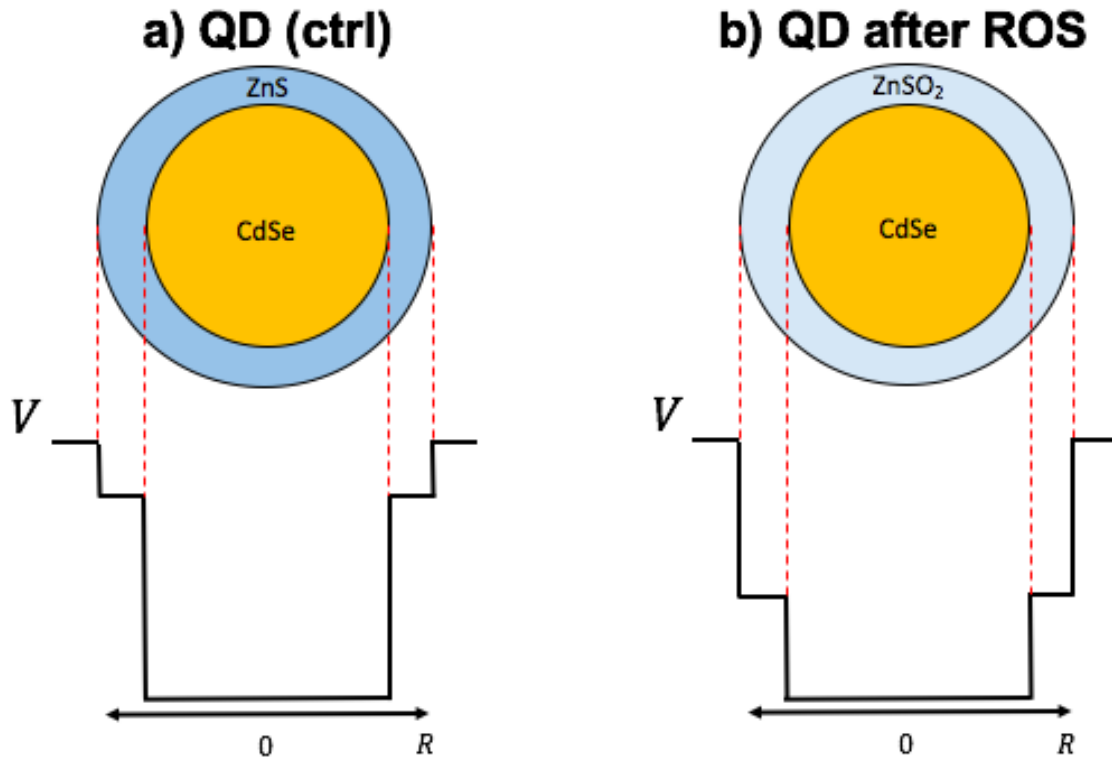


Figure 5.2: **Second Possible Mechanism.** Bioactive molecules such as ROS change the crystal structure of ZnS into $ZnSO_2$ and as a consequence changing the original 1D finite built-in potential well of CdSe/ZnS QD.

These possible mechanisms call for a time dependent study of the built-in potential well of our QD system. Slight perturbations are applied to the QD system to gradually provide an approximation to the numerical solutions of the PDE.

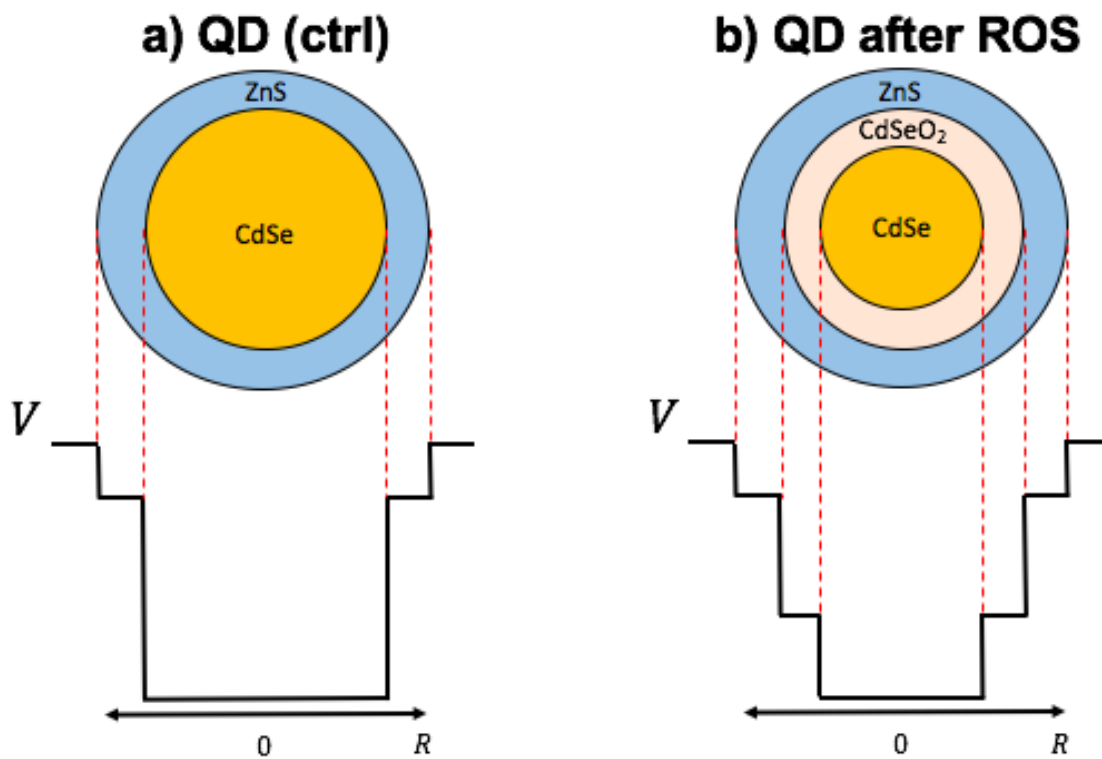


Figure 5.3: **Third Possible Mechanism.** Bioactive molecules such as ROS change the crystal structure of CdSe into $CdSeO_2$ by diffusing through ZnS or directly change the structure of CdSe due to the presence of surface defects. These processes also change the original 1D finite built-in potential well of CdSe/ZnS QD.

5.1.7 Limitations and Suggestions for Future Experiments

1. Concentration was kept at just one value for Dox, Dauno (the clinically relevant value). Dose-dependence of the result was not tested. This could be done in future.
2. X-Ray dosage was varied only for T98G as shown in appendix G. It could be varied for HL60 and K562 as well.
3. Complementary standard measurements of ROS were not done. ROS is really hard to measure but this could be done in future.
4. Patch clamp experiments can be done to establish single-cell level precision for the results.
5. Investigating the enhancement in fluorescence intensity by bioactive molecules should be undertaken in the future.
6. Addition of SOD to the chemotherapeutic experiments without cells if done, can confirm our explanation of the differences and similarities between Dox/Dauno experiments with cells and without cells.

5.1.8 Conclusions

From the hypothesis, this work raised the question whether bioactive molecules and cytomolecular products might alter the photophysical properties of QDs. Well known results such as H_2O_2 induced modulation of QD intensity were obtained in this work, to confirm the reliability of our setup. Novel results from this work include the highly significant modulation of the photophysical properties of PEGylated CdSe/ZnS by bioactive molecules in therapeutic concentrations of Dox and Dauno. This suggests using PEGylated QDs and similar conjugates as biophysical assays for characterizing ROS production in the context of NPDD. Furthermore, this work

showed that molecules from cells such as ROS, modulate the opto-electronic properties of QDs. Different cell types can possibly be mimicked technologically when both optical enhancement and attenuation are desired (as with T98G) and when only optical quenching or attenuation is desired. These applications might appear far away, but the proof of concept is already demonstrated in this work.

Appendix A

Published Abstracts

American Physical Society March Meeting 2018, Los Angeles, CA, U.S.A.

Optoelectronic Tuning of Quantum Dots by Biological Cells. Bong Han Lee, Dept of Physics, Creighton University, Sindhuja Suresh, Dept of Computer Science, Creighton University, Andrew Ekpenyong, Dept of Physics, Creighton University

Quantum dots (QDs) have applications and promising myriad applications in photovoltaic cells, biomedical imaging, targeted drug delivery, and quantum information processing. These have led to much research on their interactions with other systems. For biological systems, research has focused on the biocompatibility and cytotoxicity of QDs in the context of imaging/therapy. However, there is a paucity of work on how biological systems might be used to alter the optoelectronic properties of QDs. Here, we show that these properties can be altered by biological macromolecules following controlled changes in cellular activities. Using CdSe/ZnS core-shell QDs, spectroscopic analysis of optically excited colloidal QDs with HL60, K562, and HCN2 cell lines are performed. Our results show statistically significant ($p < 0.0001$) quenching of the emission spectra of the colloidal dispersions due to the reactive oxygen species (ROS) produced by these cells following chemotherapy and radiotherapy. This optical

modulation constitutes what we describe as cyto-molecular tuning. This type of tuning will possibly enhance applications of QDs in green energy and biomedical imaging.

American Physical Society March Meeting 2017, New Orleans, LO, U.S.A

Cyto-molecular Tuning of Quantum Dots. Bong Lee, Dept of Physics, Creighton University, Sindhuja Suresh, Dept of Computer Science, Creighton University, Andrew Ekpenyong, Dept of Physics, Creighton University

Quantum dots (QDs) are semiconductor nanoparticles composed of groups II–VI or III–V elements, with physical dimensions smaller than the exciton Bohr radius, and between 1-10 nm. Their applications and promising myriad applications in photovoltaic cells, biomedical imaging, targeted drug delivery, quantum computing, etc, have led to much research on their interactions with other systems. For biological systems, research has focused on biocompatibility and cytotoxicity of QDs in the context of imaging/therapy. However, there is a paucity of work on how biological systems might be used to tune QDs. Here, we hypothesize that the photo-electronic properties of QDs can be tuned by biological macromolecules following controlled changes in cellular activities. Using CdSe/ZnS core-shell QDs, we perform spectroscopic analysis of optically excited colloidal QDs with and without promyelocytic HL60 cells. Preliminary results show shifts in the emission spectra of the colloidal dispersions with and without cells. We will present results for activated HL60-derived cells where specific macromolecules produced by these cells perturb the electric dipole moments of the excited QDs and the associated electric fields, in ways that constitute what we describe as cyto-molecular tuning.

Biophysical Meeting 2018, San Francisco, CA, U.S.A.

Effects of Ionizing Radiation on the Mechanosensitivity of Single Cells.

Andrew E. Ekpenyong, Michael Mimplitz, Noah Zetocha, Kaamil Abid, Bong Han Lee. Physics, Creighton University, Omaha, NE, USA

The relationship between radiosensitivity and mechanosensitivity, two separate properties of cells, tissues and organs that are both important in cancer, is unclear. Radiosensitivity- the relative susceptibility to the harmful effects of ionizing radiation, is the decisive factor used in radiation therapy. Mechanosensitivity- the specific response to mechanical stimuli such as forces, depends on the mechanical properties of cells themselves which have been used, inter alia, in mechanophenotyping for cancer diagnosis. Here, we show a relationship between radiosensitivity and mechanosensitivity at the single cell level. We used a microfluidic microcirculation mimetic (MMM) which mimics the capillary constrictions of the pulmonary and peripheral microcirculation, to determine if in-vivo-like mechanical stimuli can evoke different responses from cells subjected to low dose and high dose ionizing radiation by means of radiotherapy-grade cell irradiator (CellRad, Faxitron). We also used migration assays and CdSe/ZnS core-shell nanoparticles (quantum dots) to quantify functional changes in cells following radiotherapy and MMM advection. The transit times of cells K562 (erythroid) and HL60 (myeloid) cells advected through the MMM were altered by the X-rays. Our results are first steps in evaluating the pro-metastatic effects of radiotherapy based on their induced alterations in cell mechanosensitivity, potentially providing a new rationale for the improvement of radiotherapy protocols.

American Association of Physicists in Medicine Meeting 2017, Denver, CO, U.S.A.

Radiotherapy and Chemotherapy Promote Metastasis Before Cell Death by Altering Cell Mechanical Properties. N Zetocha , B Lee , S Prathivadhi-Bhayankaram , M Mimlitz , A Ekpenyong*, Creighton University, Omaha, NE

Purpose: Although radiotherapy and chemotherapy target the proliferation of cancer cells, it is metastasis that leads to over 90% of all cancer deaths. Surprisingly, there is emerging clinical and scientific evidence that certain anti-cancer drugs as well as low dose ionizing radiation can actually promote metastasis, but the mechanisms behind their pro-metastatic effects are not completely known. Here, we seek to determine if the mechanical properties of cells subjected to various cancer drugs and radiotherapy are altered in ways that inadvertently promote metastasis.

Methods: We used a microfluidic microcirculation platform which mimics the capillary constrictions of the pulmonary and peripheral microcirculation, to apply in-vivo-like mechanical stimuli on the cells. We also used migration assays and CdSe/ZnS core-shell nanoparticles (quantum dots) to spectroscopically quantify functional changes in cells following chemotherapy and radiotherapy.

Results: We found that leukemic cancer cells treated with doxorubicin and daunorubicin, commonly used anti-cancer drugs, have over 100% longer transit times through the device, compared to untreated leukemic cells. Such delays in the microcirculation are known to promote extravasation of cells, a key step in the metastatic cascade. Furthermore, there was a significant ($p < 0.01$) increase in the chemotactic migration of the doxorubicin treated leukemic cells. We have extended our microfluidic microcirculation mimetic (MMM) to include the advection of cancer cells irradiated with

gamma photons from Co-60 and UV photons.

Conclusion: Both enhanced retention in the microcirculation and enhanced migration following chemotherapy, which we have discovered, are pro-metastatic effects which can serve as new targets for anti-metastatic drugs. For radiotherapy, our results are first steps in evaluating the pro-metastatic effects of low dose irradiation based on their induced alterations in cell mechanical properties, potentially providing a new rationale for the improvement of radiotherapy protocols.

Nebraska Academy of Sciences Meeting 2018, Lincoln, NE, U.S.A.

Optoelectronic Modulation Of Quantum Dots By Biological Cells. Bong Han Lee, Sindhuja Suresh, Andrew Ekpenyong, Creighton University, Omaha, NE

Quantum dots (QDs) have applications and promising myriad applications in photovoltaic cells, biomedical imaging, targeted drug delivery, and quantum information processing. These have led to much research on their interactions with other systems. For biological systems, research has focused on the biocompatibility and cytotoxicity of QDs in the context of imaging/therapy. However, there is a paucity of work on how biological systems might be used to alter the optoelectronic properties of QDs. Here, we show that these properties can be altered by biological macromolecules following controlled changes in cellular activities. Using CdSe/ZnS core-shell QDs, spectroscopic analysis of optically excited colloidal QDs with HL60, K562, and HCN2 cell lines are performed. Our results show statistically significant ($p < 0.0001$) quenching of the emission spectra of the colloidal dispersions due to the reactive oxygen species (ROS) produced by these cells following chemotherapy and radiotherapy. This optical modulation constitutes what we describe as cyto-molecular tuning. This type

of tuning will possibly enhance applications of QDs in green energy and biomedical imaging.

Appendix B

Published/Submitted Journal Articles

1. B. Lee, S. Suresh, A. Ekpenyong. Fluorescence Intensity Modulation of CdSe/ZnS Quantum Dots Assesses ROS During Chemotherapy and Radiotherapy for Cancer Cells. *Journal of Biophotonics*, 2018. “(Under Review)”.

Appendix C

Cell Culture Protocols

Culturing HL60 Cells

Following the cell culture method provided by HL-60 (ATCC[®] CCL-240[™]),

1. Turn on water bath and set the temperature control at 37°C.
2. Place RPMI from the refrigerator to the water bath. The temperature of the water bath does not need to be at 37°C initially.
3. Put on gloves and sterilize the hood and equipment with 75% ethanol.
4. Use the same towel to wipe.
5. Take out from the inventory the following:

Quantity	Item
1	5 mL Glass Rod
1	10 mL Glass Rod
1	Plastic Pippet
1	hemocytometer Set
1	Mechanical Counter
1	T25 Flask
1	10 μ l Mechanical Pipette
1	Set of Pipette Tips

6. These items must be airtight prior to use.
7. Sterilize microscope stand.
8. Sterilize hemocytometer.
9. Take out cells from the incubator. Do not open the incubator fully.
10. Take a look of them with a microscope.
11. Take out cells with pipette and place it within a small vial (does not necessarily have to be sterilized).
12. Use 10 ul yellow tip and place it at the ends of the hemocytomter. It should be 5 ul on each end of the hemocytometer.
13. Place the hemocytometer on the microscope stand and set the microscope at 10X.
14. The hemocytometer will contain 4 quadrants, where they are located in the following manner.

The first quadrant (Q1) is located at the top left corner.

The second quadrant (Q2) is located at the top right corner.

The third quadrant (Q3) is located at the bottom left corner.

The fourth quadrant (Q4) is located at the bottom right corner.

15. Using the mechanical counter, count the number of cells in each quadrant from right to left going downwards as in the shape of a snake.
16. Take the average of the number of cells from each quadrant and multiply it times 10^4 .
17. Use the the following equation to determine the Cell Density Average.

$$\text{Cell Density Average} = \left(\frac{Q1+Q2+Q3+Q4}{4} \right) \times 10^4$$

18. The number of cells per mL should be in between 200,000 (min) to 1,000,000 (max).
19. If the initial concentration, C_1 happen to be greater than 200,000 $\frac{\text{cells}}{\text{mL}}$, adjust the ratio of cell (A) to cells and medium (B) and produce a final concentration, C_f that is at 200,000 $\frac{\text{cells}}{\text{mL}}$.

$$C_1V_1 = C_2V_2$$

20. Dilute cells.
21. Incubate culture at 37°C.
22. Cell feeding occurs every 3 times a week.

Culturing K562 Cells

Following the cell culture method provided by K-562 (ATCC® CCL-243™), the same protocol for culturing HL60 cells are used for K562 cells.

Culturing T98G Cells

Following the cell culture method provided by T98G [T98-G] (ATCC® CRL-1690™),

1. Replace the old medium (EMEM 10% FPS).
2. Rinse with Dulbecco's Phosphate Buffered Saline, DPB.
3. Add .5 mL Trypsin-EDTA solution to lift cell from flask.
4. Incubate the flask at 37°C for 5 min.
5. Add 5 mL of medium to deactivate Trypsin-EDTA solution.
6. Dilute the cell by 1 mL.
7. Centrifuge with 900 RPM for 5 min.
8. Add medium once again.
9. Incubate culture at 37°C.
10. Cell feeding occurs every 3 times a week.

Appendix D

Spectroscopic Protocols

Protocol for mixing colloidal solution of hydrophilic CdSe/ZnS QDs onto H_2O_2 .

1. Prepare the stock for QD of 4 μ M by taking 100 μ l and add it into 2.5 ml of deionized water to create a stock concentration of 0.1538 μ M.
2. For 0% H_2O_2 (516813-500ML Sigma Aldrich), take 520 μ l of stock solution of QD and add it into the cuvette.
3. For 0.1% H_2O_2 , take 520 μ l of stock solution of QD, 1.04 μ l of H_2O_2 , and add them into the cuvette.
4. For 1% H_2O_2 , take 518.96 μ l of stock solution of QD, 10.4 μ l of H_2O_2 , and add them into the cuvette.
5. For 5% H_2O_2 , take 509.6 μ l of stock solution of QD 52 μ l of H_2O_2 , and add them into the cuvette.
6. For 10% H_2O_2 , take 468 μ l of stock solution of QD 104 μ l of H_2O_2 , and add them into the cuvette.

Protocol for mixing colloidal solution of hydrophilic CdSe/ZnS QDs with cells.

1. To add QDs onto cells, disinfect the hood before starting the experiment, and prepare a curvette holder.
2. When using the mechanical pipette, use the blue pipette tip for the stock of cells.
3. Press the plunger halfway of the mechanical pipette to extract 500 ul solution of cells.
4. Release the plunger to release the solution of cells onto the curvettes.
5. Change the tip of the mechanical pipette with the yellow pipette tip.
6. Press the plunger halfway to extract 20 ul solution from 4 uM concentration of QD to create a final concentration of 0.1538 uM.
7. Release the plunger to release the solution of QD onto the curvettes.
8. Press the plunger halfway 15 times to mix the combined solution of cells and QD.
9. Cover the curvettes with a plastic membrane.
10. Cover the curvette holder with a black felt.
11. Disinfect the hood after finishing the experiment.

Protocol for mixing colloidal solution of hydrophilic CdSe/ZnS QDs with medium and chemotherapeutic Drugs

1. Take out Doxorubicin and Daunorubicin out of the freezer.
2. In 2 X T25 flasks, add 5 mL of RPMI to each of them.

3. For a final concentration of 5 μM of Doxorubicin (4458 Sigma), take 25 μl of Doxorubicin with an initial concentration of 1 mM , and add it to one of the T25 flask.
4. For a final concentration of 1 μM of Daunorubicin (D8809 Sigma), take 25 μl of Daunorubicin with an initial concentration of 0.2 mM , and add it to the other T25 flask.
5. Take 500 μl from each of the T25 flasks and add them to the cuvettes.
6. Add 20 μl of hydrophilic CdSe/ZnS QDs to each of them.

Protocol for mixing colloidal solution of hydrophilic CdSe/ZnS QDs with cells treated with chemotherapeutic Drugs

1. Take out Doxorubicin and Daunorubicin out of the freezer.
2. In 2 X T25 flasks, add 5 mL of either cells to each of them.
3. For a final concentration of 5 μM of Doxorubicin (4458 Sigma), take 25 μl of Doxorubicin with an initial concentration of 1 mM , and add it to one of the T25 flask.
4. For a final concentration of 1 μM of Daunorubicin (D8809 Sigma), take 25 μl of Daunorubicin with an initial concentration of 0.2 mM , and add it to the other T25 flask.
5. Take 500 μl from each of the T25 flasks and add them to the cuvettes.
6. Add 20 μl of hydrophilic CdSe/ZnS QDs to each of them.

Protocol for mixing colloidal solution of hydrophilic CdSe/ZnS QDs with cells treated with radiotherapy

1. Warm up Faxitron CellRad.
2. Add the cell culture that are in T25 flask into Faxitron CellRad.
3. Press automatical dose control mode to input the desired dose onto the cell culture.
4. Take 500 ul from each of the T25 flask and add them to the cuvettes.
5. Add 20 ul of hydrophilic CdSe/ZnS QDs to each of them.

Appendix E

COMSOL Codes

Simulation Logs

```

===== Simulation for Electron in QD Well=====
Number of vertex elements: 12
Number of edge elements: 288
Number of boundary elements: 5202
Number of elements: 51079
Free meshing time: 1.23s
Minimum element quality: 0.234
<---- Compile Equations: Eigenvalue in Study 1/Solution 1 (sol1)
Started at 11-Jul-2018 00:16:55.
Geometry shape order: Quadratic
Running on Intel(R) Core(TM) i5-2520M CPU at 2.50 GHz.
Using 2 cores on 1 socket.
Available memory: 3.98 GB.
Time: 1 s.
Physical memory: 1.07 GB
Virtual memory: 1.21 GB
Ended at 11-Jul-2018 00:16:56.
Compile Equations: Eigenvalue in Study 1/Solution 1 (sol1)---->
<---- Eigenvalue Solver 1 in Study 1/Solution 1 (sol1)
Started at 11-Jul-2018 00:16:57.
Eigenvalue solver
Number of degrees of freedom solved for: 70950 (plus 16696 internal
DOFs).
Symmetric matrices found.
Scales for dependent variables:
Dependent variable u (comp1.u): 1
Orthonormal null-space function used.
Symmetric eigenvalue solver.
Iter      ErrEst  Nconv
   1      0.12   0
   2      0.094  1
   3      0.031  1
   4       0.3   1
   5      0.0038  1
   6      5.4e-005  1
   7      5.1e-006  1
   8       0.21  3
   9      0.038  1
  10      0.003  1
  11     0.00014  1
  12     1.2e-005  1
  13     7.4e-007  4
45 linear system solutions.
146 matrix multiplications.
44 re-orthogonalizations.
Solution time: 16 s.
Physical memory: 1.45 GB
Virtual memory: 1.64 GB
Ended at 11-Jul-2018 00:17:13.
----- Eigenvalue Solver 1 in Study 1/Solution 1 (sol1) ----->

```

```

===== Simulation for Hole in QD Well =====
<---- Compile Equations: Eigenvalue in Study 1/Solution 1 (sol1)
Started at 11-Jul-2018 00:43:14.
Geometry shape order: Quadratic
Running on Intel(R) Core(TM) i5-2520M CPU at 2.50 GHz.
Using 2 cores on 1 socket.
Available memory: 3.98 GB.
Time: 1 s.
Physical memory: 930 MB
Virtual memory: 1049 MB
Ended at 11-Jul-2018 00:43:15.
Compile Equations: Eigenvalue in Study 1/Solution 1 (sol1)---->
<---- Eigenvalue Solver 1 in Study 1/Solution 1 (sol1)
Started at 11-Jul-2018 00:43:16.
Eigenvalue solver
Number of degrees of freedom solved for: 70950 (plus 16696 internal
DOFs).
Symmetric matrices found.
Scales for dependent variables:
Dependent variable u (comp1.u): 1
Orthonormal null-space function used.
Symmetric eigenvalue solver.
Iter      ErrEst  Nconv
  1         0.15    0
  2         0.047   1
  3         0.011   1
  4         0.029   1
  5         0.00024  1
  6         1.1e-005  1
  7          0.16   1
  8         0.0037  1
  9         0.00015  1
 10         6.6e-006  1
 11         3.7e-007  4
40 linear system solutions.
129 matrix multiplications.
39 re-orthogonalizations.
Solution time: 15 s.
Physical memory: 1.35 GB
Virtual memory: 1.49 GB
Ended at 11-Jul-2018 00:43:31.
----- Eigenvalue Solver 1 in Study 1/Solution 1 (sol1)----->

```

Appendix F

Copyright Permissions

**JOHN WILEY AND SONS LICENSE
TERMS AND CONDITIONS**

Aug 05, 2018

This Agreement between Mr. Bong Han Lee ("You") and John Wiley and Sons ("John Wiley and Sons") consists of your license details and the terms and conditions provided by John Wiley and Sons and Copyright Clearance Center.

License Number	4402650272135
License date	Aug 05, 2018
Licensed Content Publisher	John Wiley and Sons
Licensed Content Publication	Wiley Books
Licensed Content Title	Fundamentals of Materials Science and Engineering: An Integrated Approach, 4th Edition
Licensed Content Author	David G. Rethwisch William D. Callister
Licensed Content Date	Nov 1, 2011
Licensed Content Pages	1
Type of use	Dissertation/Thesis
Requestor type	University/Academic
Format	Print and electronic
Portion	Figure/table
Number of figures/tables	1
Original Wiley figure/table number(s)	Figure 18.3
Will you be translating?	No
Title of your thesis / dissertation	OPTO-ELECTRONIC MODULATION OF QUANTUM DOTS BY CELLS AND BIOACTIVE MOLECULES
Expected completion date	Jul 2018
Expected size (number of pages)	70
Requestor Location	Mr. Bong Han Lee 3660 Cass St OMAHA, NE 68131 United States Attn: Mr. Bong Han Lee
Publisher Tax ID	EU826007151
Total	0.00 USD
Terms and Conditions	

TERMS AND CONDITIONS

This copyrighted material is owned by or exclusively licensed to John Wiley & Sons, Inc. or one of its group companies (each a "Wiley Company") or handled on behalf of a society with which a Wiley Company has exclusive publishing rights in relation to a particular work (collectively "WILEY"). By clicking "accept" in connection with completing this licensing transaction, you agree that the following terms and conditions apply to this transaction

**JOHN WILEY AND SONS LICENSE
TERMS AND CONDITIONS**

Aug 05, 2018

This Agreement between Mr. Bong Han Lee ("You") and John Wiley and Sons ("John Wiley and Sons") consists of your license details and the terms and conditions provided by John Wiley and Sons and Copyright Clearance Center.

License Number	4402660568985
License date	Aug 05, 2018
Licensed Content Publisher	John Wiley and Sons
Licensed Content Publication	Wiley Books
Licensed Content Title	Quantum Dots
Licensed Content Author	Wolfgang Johann Parak, Liberato Manna, Friedrich C. Simmel, et al
Licensed Content Date	Sep 3, 2010
Licensed Content Pages	45
Type of use	Dissertation/Thesis
Requestor type	University/Academic
Format	Print and electronic
Portion	Figure/table
Number of figures/tables	1
Original Wiley figure/table number(s)	Figure 2.11
Will you be translating?	No
Title of your thesis / dissertation	OPTO-ELECTRONIC MODULATION OF QUANTUM DOTS BY CELLS AND BIOACTIVE MOLECULES
Expected completion date	Jul 2018
Expected size (number of pages)	70
Requestor Location	Mr. Bong Han Lee 3660 Cass St OMAHA, NE 68131 United States Attn: Mr. Bong Han Lee
Publisher Tax ID	EU826007151
Total	0.00 USD
Terms and Conditions	

TERMS AND CONDITIONS

This copyrighted material is owned by or exclusively licensed to John Wiley & Sons, Inc. or one of its group companies (each a "Wiley Company") or handled on behalf of a society with which a Wiley Company has exclusive publishing rights in relation to a particular work (collectively "WILEY"). By clicking "accept" in connection with completing this licensing transaction, you agree that the following terms and conditions apply to this transaction (along with the billing and payment terms and conditions established by the Copyright

**SPRINGER NATURE LICENSE
TERMS AND CONDITIONS**

Jun 25, 2018

This Agreement between Mr. Bong Han Lee ("You") and Springer Nature ("Springer Nature") consists of your license details and the terms and conditions provided by Springer Nature and Copyright Clearance Center.

License Number	4376071233480
License date	Jun 25, 2018
Licensed Content Publisher	Springer Nature
Licensed Content Publication	Nature Materials
Licensed Content Title	Quantum dot bioconjugates for imaging, labelling and sensing
Licensed Content Author	Igor L. Medintz, H. Tetsuo Uyeda, Ellen R. Goldman, Hedi Mattoussi
Licensed Content Date	Jun 1, 2005
Licensed Content Volume	4
Licensed Content Issue	6
Type of Use	Thesis/Dissertation
Requestor type	academic/university or research institute
Format	print and electronic
Portion	figures/tables/illustrations
Number of figures/tables/illustrations	1
High-res required	no
Will you be translating?	no
Circulation/distribution	2,001 to 5,000
Author of this Springer Nature content	no
Title	OPTO-ELECTRONIC MODULATION OF QUANTUM DOTS BY CELLS AND BIOACTIVE MOLECULES
Instructor name	n/a
Institution name	n/a
Expected presentation date	Jul 2018
Portions	Figure 2 (d) only
Requestor Location	Mr. Bong Han Lee 3660 Cass St OMAHA, NE 68131 United States Attn: Mr. Bong Han Lee
Billing Type	Invoice
Billing Address	Mr. Bong Han Lee 3660 Cass St

Appendix G

List of Experiments

Table G.1 shows the complete list of experiments done in this research. For the case of T98G cells treated with 2 Gy X-Rays, results were inconclusive as only one experiment had been done with it as N1.

Experiment	Cell Line	Controlled Changes
Hydrophobic CdSe/ZnS QD (Control)	N.A.	Hydrophobic CdSe/ZnS QD with an emission peak at 540 ± 10 nm
Hydrophilic CdSe/ZnS QD (Control)	N.A.	Hydrophilic CdSe/ZnS QD with an emission at emission peak at 540 ± 10 nm
H_2O_2	N.A.	Concentrations of 0%, 0.1%, 1%, 5%, 10%
Chemotherapy and Medium	N.A.	Chemotherapeutic drugs: Dauno and Dox
Chemotherapy	HL60	Chemotherapeutic drugs: Dauno and Dox
Chemotherapy	K562	Chemotherapeutic drugs: Dauno and Dox
Radiotherapy	HL60	20 Gy X-Ray. Measurement done 1 hr post radiotherapy
Radiotherapy	K562	20 Gy X-Ray. Measurement done 1 hr post radiotherapy
Radiotherapy	T98G	2 and 20 Gy X-Ray. Measurement done 1 hr post radiotherapy
X-Ray	T98G	2 Gy X-Ray. Measurement done 1 hr post radiotherapy

Table G.1: Complete List of Experimental Conditions. Nine experimental conditions along with their descriptions. The first two experiment conditions serve as control variables, and the rest of the experimental conditions had CdSe/ZnS QDs introduced after the controlled changes.

Bibliography

- [1] Finite Element Method. <https://www.comsol.com/multiphysics/finite-element-method>. Accessed: 2018-04-29.
- [2] How can I reduce noise in my Spectra? <https://oceanoptics.com/faq/can-reduce-noise-spectra/>. Accessed: 2018-04-29.
- [3] Introduction to Comsol Multiphysics. <https://cdn.comsol.com/documentation/5.3.0.316/IntroductionToCOMSOLMultiphysics.pdf>. Accessed: 2018-04-29.
- [4] Mesh Refinement. <https://www.comsol.com/multiphysics/mesh-refinement>. Accessed: 2018-04-29.
- [5] Optical Properties of Quantum Dots: An Undergraduate Physics Laboratory. <https://web.wpi.edu/Pubs/E-project/Available/E-project-042607-125225/unrestricted/QuantumDots.pdf>. Accessed: 2017-01-29.
- [6] Product Specification. https://www.sigmaaldrich.com/Graphics/COFAInfo/SigmaSAPQM/SPEC/90/900244/900244-BULK_____ALDRICH__.pdf. Accessed: 2018-08-07.

- [7] Solving Nonlinear Static Finite Element Problems. <https://www.comsol.com/blogs/solving-nonlinear-static-finite-element-problems/>. Accessed: 2018-04-29.
- [8] T98G (ATCC CRL-1690). <https://www.atcc.org/Products/All/CRL-1690.aspx#generalinformation>. Accessed: 2018-04-29.
- [9] Thawing, Propagation and Cryopreservation of NCI-PBCF-CRL1690 (T98G). https://physics.cancer.gov/docs/bioresource/brain/NCI-PBCF-CRL1690_T98G_SOP-508.pdf. Accessed: 2018-08-04.
- [10] W Russ Algar, Ani Khachatrian, Joseph S Melinger, Alan L Huston, Michael H Stewart, Kimihiro Susumu, Juan B Blanco-Canosa, Eunkeu Oh, Philip E Dawson, and Igor L Medintz. Concurrent Modulation of Quantum Dot Photoluminescence Using a Combination of Charge Transfer and Forster Resonance Energy Transfer: Competitive Quenching and Multiplexed Biosensing Modality. *Journal of the American Chemical Society*, 139(1):363–372, 2016.
- [11] A. P. Alivisatos. Semiconductor Clusters, Nanocrystals, and Quantum Dots. *American Association for the Advancement of Science*, 271(5251):933–937, 1996.
- [12] Gholam Reza Amiri, Soheil Fatahian, and Somayeh Mahmoudi. Preparation and Optical Properties Assessment of CdSe Quantum Dots. *Materials Sciences and Applications*, 4(2):134, 2013.
- [13] Holly E Barker, James TE Paget, Aadil A Khan, and Kevin J Harrington. The Tumour Microenvironment After Radiotherapy: Mechanisms of Resistance and Recurrence. *Nature Reviews Cancer*, 15(7):409, 2015.
- [14] Sotirios Baskoutas and Andreas F Terzis. Size-Dependent Band Gap of Colloidal Quantum Dots. *J. Appl. Phys.*, 99(013708):1–4, 2006.

- [15] Mounji G Bawendi, Michael L Steigerwald, and Louis E Brus. The Quantum Mechanics of Larger Semiconductor Clusters (“Quantum Dots”). *Annual Review of Physical Chemistry*, 41(1):477–496, 1990.
- [16] Karl Brehwens. *In Vitro and in Vivo Aspects of Intrinsic Radiosensitivity*. PhD thesis, Department of Molecular Biosciences, the Wenner-Gren Institute, 2014.
- [17] Louis Brus. Electronic Wave Functions in Semiconductor Clusters: Experiment and Theory. *The Journal of Physical Chemistry*, 90(12):2555–2560, 1986.
- [18] Louis E Brus. Electron-Electron and Electron-Hole Interactions in Small Semiconductor Crystallites: The Size Dependence of the Lowest Excited Electronic State. *The Journal of Chemical Physics*, 80(9):4403–4409, 1984.
- [19] Clare Bryant and Katherine A Fitzgerald. Molecular Mechanisms Involved in Inflammasome Activation. *Trends in Cell Biology*, 19(9):455–464, 2009.
- [20] Xiaoli Cai, Yanan Luo, Weiyang Zhang, Dan Du, and Yuehe Lin. pH-Sensitive ZnO Quantum Dots–Doxorubicin Nanoparticles for Lung Cancer Targeted Drug Delivery. *ACS Applied Materials & Interfaces*, 8(34):22442–22450, 2016.
- [21] William D Callister Jr and David G Rethwisch. *Fundamentals of Materials Science and Engineering: An Integrated Approach*. John Wiley & Sons, 4th edition, 2012.
- [22] Krishnan V Chakravarthy, Bruce A Davidson, Jadwiga D Helinski, Hong Ding, Wing-Cheung Law, Ken-Tye Yong, Paras N Prasad, and Paul R Knight. Doxorubicin-Conjugated Quantum Dots to Target Alveolar Macrophages and Inflammation. *Nanomedicine: Nanotechnology, Biology and Medicine*, 7(1):88–96, 2011.

- [23] Cheng-Shane Chu, Meng-Wei Hsieh, and Zhi-Ren Su. Optical Sensing of H_2O_2 Based on Red-Shift of Emission Wavelength of Carbon Quantum Dots. *Optical Materials Express*, 6(3):759–766, 2016.
- [24] Steven J Collins. The HL-60 Promyelocytic Leukemia Cell Line: Proliferation, Differentiation, and Cellular Oncogene Expression. *Blood*, 70(5):1233–1244, 1987.
- [25] Bashir O Dabbousi, Javier Rodriguez-Viejo, Frederic V Mikulec, Jason R Heine, Hedi Mattoussi, Raymond Ober, Klavs F Jensen, and Mounji G Bawendi. (CdSe) ZnS Core-Shell Quantum Dots: Synthesis and Characterization of a Size Series of Highly Luminescent Nanocrystallites. *The Journal of Physical Chemistry B*, 101(46):9463–9475, 1997.
- [26] Antonella De Angelis, Konrad Urbanek, Donato Cappetta, Elena Piegari, Loreta Pia Ciuffreda, Alessia Rivellino, Rosa Russo, Grazia Esposito, Francesco Rossi, and Liberato Berrino. Doxorubicin Cardiotoxicity and Target Cells: A Broader Perspective. *Cardio-Oncology*, 2(1):2, 2016.
- [27] TPA Devasagayam, JC Tilak, KK Bloor, Ketaki S Sane, Saroj S Ghaskadbi, and RD Lele. Free Radicals and Antioxidants in Human Health: Current Status and Future Prospects. *Japi*, 52(794804):4, 2004.
- [28] A.I. Ekimov, Al.L. Efros, and A.A. Onushchenko. Quantum Size Effect in Semiconductor Microcrystals. *Solid State Communications*, 88(11):947–950, 1993.
- [29] Andrew E Ekpenyong, Graeme Whyte, Kevin Chalut, Stefano Pagliara, Franziska Lautenschläger, Christine Fiddler, Stephan Paschke, Ulrich F Keyser, Edwin R Chilvers, and Jochen Guck. Viscoelastic Properties of Differentiating Blood Cells are Fate and Function-Dependent. *PLoS ONE*, 7(9):e45237, 2012.

- [30] Peter P Fu, Qingsu Xia, Huey-Min Hwang, Paresh C Ray, and Hongtao Yu. Mechanisms of Nanotoxicity: Generation of Reactive Oxygen Species. *Journal of Food and Drug Analysis*, 22(1):64–75, 2014.
- [31] Zhixing Gan, Qingfeng Gui, Yun Shan, Pengfei Pan, Ning Zhang, and Lifa Zhang. Photoluminescence of MoS₂ Quantum Dots Quenched by Hydrogen Peroxide: A Fluorescent Sensor for Hydrogen Peroxide. *Journal of Applied Physics*, 120(10):104503, 2016.
- [32] Kathy K Griendling, Rhian M Touyz, Jay L Zweier, Sergey Dikalov, William Chilian, Yeong-Renn Chen, David G Harrison, and Aruni Bhatnagar. Measurement of Reactive Oxygen Species, Reactive Nitrogen Species, and Redox-Dependent Signaling in the Cardiovascular System: A Scientific Statement From the American Heart Association. *Circulation Research*, 119(5):e39–e75, 2016.
- [33] David J Griffiths and Darrell F Schroeter. *Introduction to Quantum Mechanics*. Cambridge University Press, 2nd edition, 2015.
- [34] Xi Tao Guo, Zhen Hua Ni, Chun Yan Liao, Hai Yan Nan, Yan Zhang, Wei Wei Zhao, and Wen Hui Wang. Fluorescence Quenching of CdSe Quantum Dots on Graphene. *Applied Physics Letters*, 103(20):201909, 2013.
- [35] Thomas Hartsfield, Wei-Shun Chang, Seung-Cheol Yang, Tzuhsuan Ma, Jinwei Shi, Liuyang Sun, Gennady Shvets, Stephan Link, and Xiaoqin Li. Single Quantum Dot Controls a Plasmonic Cavity’s Scattering and Anisotropy. *Proceedings of the National Academy of Sciences*, 112(40):12288–12292, 2015.
- [36] Niko Hildebrandt, Christopher M Spillmann, W Russ Algar, Thomas Pons, Michael H Stewart, Eunkeu Oh, Kimihiro Susumu, Sebastian A Diaz, James B Delehanty, and Igor L Medintz. Energy Transfer With Semiconductor Quantum

- Dot Bioconjugates: A Versatile Platform for Biosensing, Energy Harvesting, and Other Developing Applications. *Chemical Reviews*, 117(2):536–711, 2016.
- [37] Thang B Hoang, Gleb M Akselrod, Christos Argyropoulos, Jiani Huang, David R Smith, and Maiken H Mikkelsen. Ultrafast Spontaneous Emission Source Using Plasmonic Nanoantennas. *Nature Communications*, 6:7788, 2015.
- [38] Petras Juzenas, Wei Chen, Ya-Ping Sun, Manuel Alvaro Neto Coelho, Roman Generalov, Natalia Generalova, and Ingeborg Lie Christensen. Quantum Dots and Nanoparticles for Photodynamic and Radiation Therapies of Cancer. *Advanced Drug Delivery Reviews*, 60(15):1600–1614, 2008.
- [39] Cherie R Kagan, Efrat Lifshitz, Edward H Sargent, and Dmitri V Talapin. Building Devices From Colloidal Quantum Dots. *Science*, 353(6302):aac5523, 2016.
- [40] Lillian S Kao and Charles E Green. Analysis of variance: Is There a Difference in Means and What Does it Mean? *Journal of Surgical Research*, 144(1):158–170, 2008.
- [41] Dorota Kostrzewa-Nowak, MJI Paine, CR Wolf, and J Tarasiuk. The Role of Bioreductive Activation of Doxorubicin in Cytotoxic Activity Against Leukaemia HL60-Sensitive Cell Line and its Multidrug-Resistant Sublines. *British Journal of Cancer*, 93(1):89, 2005.
- [42] Rubin H Landau, Cristian C Bordeianu, et al. *Computational Physics: Problem Solving with Python*. John Wiley & Sons, 3rd edition, 2015.
- [43] Qiangqiang Liu, Hongxia Li, Qiyue Xia, Ying Liu, and Kai Xiao. Role of Surface Charge in Determining the Biological Effects of CdSe/ZnS Quantum Dots. *International Journal of Nanomedicine*, 10:7073, 2015.

- [44] Daryl L Logan. *A First Course in the Finite Element Method*. Cengage Learning, 5th edition, 2011.
- [45] Edwin Lok, Pyay San, Van Hua, Melissa Phung, and Eric T Wong. Analysis of Physical Characteristics of Tumor Treating Fields for Human Glioblastoma. *Cancer Medicine*, 6(6):1286–1300, 2017.
- [46] Katherine Lugo, Xiaoyu Miao, Fred Rieke, and Lih Y Lin. Remote Switching of Cellular Activity and Cell Signaling Using Light in Conjunction With Quantum Dots. *Biomedical Optics Express*, 3(3):447–454, 2012.
- [47] Michael C Mancini, Brad A Kairdolf, Andrew M Smith, and Shuming Nie. Oxidative Quenching and Degradation of Polymer-Encapsulated Quantum Dots: New Insights Into the Long-Term Fate and Toxicity of Nanocrystals in Vivo. *Journal of the American Chemical Society*, 130(33):10836–10837, 2008.
- [48] Igor L Medintz, H Tetsuo Uyeda, Ellen R Goldman, and Hedi Mattoussi. Quantum Dot Bioconjugates for Imaging, Labelling and Sensing. *Nature Materials*, 4:435–446, 2005.
- [49] R V N Melnik and M Willatzen. Bandstructures of Conical Quantum Dots with Wetting Layers. *Nanotechnology*, 15(1):1–8, 2004.
- [50] X Michalet, FF Pinaud, LA Bentolila, JM Tsay, SJL Dose, JJ Li, G Sundaresan, AM Wu, SS Gambhir, and S Weiss. Quantum Dots for Live Cells, in Vivo Imaging, and Diagnostics. *Science*, 307(5709):538–544, 2005.
- [51] Luka Milas and Walter N Hittelman. Cancer Stem Cells and Tumor Response to Therapy: Current Problems and Future Prospects. *Seminars in Radiation Oncology*, 19(2):96–105, 2009.

- [52] Limor Minai, Daniella Yeheskely-Hayon, and Dvir Yelin. High Levels of Reactive Oxygen Species in Gold Nanoparticle-Targeted Cancer Cells Following Femtosecond Pulse Irradiation. *Scientific Reports*, 3:2146, 2013.
- [53] Pedro C Miranda, Abeye Mekonnen, Ricardo Salvador, and Peter J Basser. Predicting the Electric Field Distribution in the Brain for the Treatment of Glioblastoma. *Physics in Medicine & Biology*, 59(15):4137, 2014.
- [54] Sedat Nizamoglu and Hilmi Volkan Demir. Onion-like (CdSe) ZnS/CdSe/ZnS Quantum-Dot-Quantum-Well Heteronanocrystals for Investigation of Multi-Color Emission. *Optics Express*, 16(6):3515–3526, 2008.
- [55] Eunkeu Oh, Rong Liu, Andre Nel, Kelly Boeneman Gemill, Muhammad Bilal, Yoram Cohen, and Igor L Medintz. Meta-Analysis of Cellular Toxicity for Cadmium-Containing Quantum Dots. *Nature Nanotechnology*, 11(5):479, 2016.
- [56] Sruti V Prathivadhi-Bhayankaram, Jianhao Ning, Michael Mimplitz, Carolyn Taylor, Erin Gross, Michael Nichols, Jochen Guck, and Andrew E Ekpenyong. Chemotherapy Impedes in Vitro Microcirculation and Promotes Migration of Leukemic Cells with Impact on Metastasis. *Biochemical and Biophysical Research Communications*, 479(4):841–846, 2016.
- [57] Colleen R Reczek and Navdeep S Chandel. The Two Faces of Reactive Oxygen Species in Cancer. *Annual Review of Cancer Biology*, 1:79–98, 2017.
- [58] Peter Reiss, Myriam Protière, and Liang Li. Core/Shell Semiconductor Nanocrystals. *Small*, 5(2):154–168, 2009.
- [59] Markus F Renschler. The Emerging Role of Reactive Oxygen Species in Cancer Therapy. *European Journal of Cancer*, 40(13):1934–1940, 2004.

- [60] Sandra J Rosenthal, Jerry C Chang, Oleg Kovtun, James R McBride, and Ian D Tomlinson. Biocompatible Quantum Dots for Biological Applications. *Chemistry & Biology*, 18(1):10–24, 2011.
- [61] Jérôme Roy, Jean-Marie Galano, Thierry Durand, Jean-Yves Le Guennec, and Jetty Chung-Yung Lee. Physiological Role of Reactive Oxygen Species as Promoters of Natural Defenses. *The FASEB Journal*, 31(9):3729–3745, 2017.
- [62] A SalmanOgli and A Rostami. Investigation of Electronic and Optical Properties of (CdSe/ZnS/CdSe/ZnS) Quantum Dot–Quantum Well Heteronanocrystal. *Journal of Nanoparticle Research*, 13(3):1197–1205, 2011.
- [63] Gunter Schmid. *Nanoparticles*. Wiley, 2nd edition, 2004.
- [64] Andrew M Smith and Shuming Nie. Semiconductor Nanocrystals: Structure, Properties, and Band Gap Engineering. *Accounts of Chemical Research*, 43(2):190–200, 2009.
- [65] Pierre Sonveaux. ROS and Radiotherapy: More We Care. *Oncotarget*, 8(22):35482, 2017.
- [66] Marta Stojak, Lidia Mazur, Małgorzata Opydo-Chanek, Małgorzata Łukawska, and Irena Oszczapowicz. Effects of Structural Modifications of Daunorubicin on in Vitro Antileukemic Activity. *Anticancer Research*, 32(12):5271–5277, 2012.
- [67] Chao Wang, Xue Gao, and Xingguang Su. In Vitro and in Vivo Imaging With Quantum Dots. *Analytical and Bioanalytical Chemistry*, 397(4):1397–1415, 2010.
- [68] Jinping Wang, Xiaoxiao Tan, Xiaojuan Pang, Li Liu, Fengping Tan, and Nan Li. MoS₂ Quantum Dot@polyaniline Inorganic–Organic Nanohybrids for in Vivo Dual-Modal Imaging Guided Synergistic Photothermal/Radiation Therapy. *ACS Applied Materials & Interfaces*, 8(37):24331–24338, 2016.

- [69] Tomasz Wojcik, Elzbieta Buczek, Katarzyna Majzner, Agnieszka Kolodziejczyk, Justyna Miszczyk, Patrycja Kaczara, Wojciech Kwiatek, Malgorzata Baranska, Marek Szymonski, and Stefan Chlopicki. Comparative Endothelial Profiling of Doxorubicin and Daunorubicin in Cultured Endothelial Cells. *Toxicology in Vitro*, 29(3):512–521, 2015.
- [70] Hugh D. Young, Roger A. Freedman, and A. Lewis Ford. *University Physics with Modern Physics*. Pearson Education, Inc., 13th edition, 2012.
- [71] Yu Zhang, Jia He, Pei Nan Wang, Ji Yao Chen, Zhou Jun Lu, Da Ru Lu, Jia Guo, Chang Chun Wang, and Wu Li Yang. Time-Dependent Photoluminescence Blue Shift of the Quantum Dots in Living Cells: Effect of Oxidation by Singlet Oxygen. *Journal of the American Chemical Society*, 128(41):13396–13401, 2006.
- [72] Mei-Xia Zhao and Bing-Jie Zhu. The Research and Applications of Quantum Dots as Nano-Carriers for Targeted Drug Delivery and Cancer Therapy. *Nanoscale Research Letters*, 11(1):207, 2016.
- [73] Wenwan Zhong. Nanomaterials in Fluorescence-Based Biosensing. *Analytical and Bioanalytical Chemistry*, 394(1):47–59, 2009.
- [74] Pavel Zrazhevskiy and Xiaohu Gao. Multifunctional Quantum Dots for Personalized Medicine. *Nano Today*, 4(5):414–428, 2009.